M 2024

U.PORTO
FEUP FACULDADE DE ENGENHARIA
UNIVERSIDADE DO PORTO

THREE-DIMENSIONAL FUNCTIONALISED STRUCTURES FOR WATER TREATMENT

JOANA JAMBELA MATIAS DELE
MASTER THESIS IN CHEMICAL ENGINEERING
PRESENTED TO THE FACULTY OF ENGINEERING
OF THE UNIVERSITY OF PORTO

Master in Chemical Engineering

Three-dimensional functionalised structures for water treatment

Master Thesis

of

Joana Jambela Matias Dele

Developed within the course of dissertation

held in

ALiCE | Associate Laboratory in Chemical Engineering

LSRE-LCM | Laboratory of Separation and Reaction Engineering - Laboratory of Catalysis and Materials

Supervisors:

Professor Adrián M. T. Silva

Doctor André Torres-Pinto

Doctor Ana María Chávez

July of 2024

Agradecimentos

Agradeço ao Professor Adrián Silva, meu orientador, por ter me escutado e confiado em mim para a realização deste trabalho. Agradeço por todas as sugestões feitas e oportunidades oferecidas.

Ao Doutor André Torres-Pinto, meu coorientador, que esteve sempre presente e seguiu a minha trajetória com tamanha dedicação. Muito obrigada por cada segundo dedicado ao meu trabalho, por todas as vezes em que puxou por mim, por todas as correções e sugestões.

À Doutora Ana Maria Chávez, minha coorientadora, que se fez tão presente durantes esses meses, muito obrigada pela ajuda, sugestões, dedicação e preocupação.

À Professora Cláudia Silva pela disponibilidade e oportunidades oferecidas durante a realização deste trabalho.

Ao Professor Joaquim Faria, diretor do Laboratório Associado LSRE-LCM, pela disponibilização de recursos.

Ao Laboratório LSRE-LCM pela disponibilização dos seus espaços e recursos.

À Rita, Patrícia, Leonor, Sofia, Catarina, Marta, Joaquín, Márcia, Karol e Joana, agradeço por me terem acolhido e apoiado durante esses meses. Aos restantes colegas de laboratório, agradeço pela ajuda e boa disposição diária.

À Amanda, Thalita, Avelina, Carlos, Filipa e Tiffany, muito obrigada pela amizade e apoio.

À Janylza, que acompanhou cada passo desta jornada, muito obrigada por estar lá e seres a melhor.

Aos meus amigos, muito obrigado pelo apoio, amizade e companheirismo de sempre.

Finalmente, à minha mãe e ao meu pai que sempre estiveram lá e fazem o impossível para que tudo fique bem, muito obrigada. Aos meus irmãos, obrigada por serem um incentivo. À toda minha família, muito obrigada pelo apoio.

Este trabalho foi financiado por fundos nacionais através da FCT/MCTES (PIDDAC), no âmbito do projeto DRopH_2O com a referência 2022.08738.PTDC e DOI 10.54499/2022.08738.PTDC (https://doi.org/10.54499/2022.08738.PTDC), e através de LSRE-LCM, UIDB/50020/2020 (DOI: 10.54499/UIDB/50020/2020) e UIDP/50020/2020 (DOI: 10.54499/UIDP/50020/2020); e ALiCE, LA/P/0045/2020 (DOI: 10.54499/LA/P/0045/2020).

fct Fundação para a Ciência e a Tecnologia

REPÚBLICA PORTUGUESA

Abstract

The development and optimisation of technologies for water treatment are more and more needed due to the increasing levels of organic micropollutants found in water matrices, including drinking water. Adsorption is one of the simplest treatment processes that can be applied to remove micropollutants from water and several adsorbents have been developed, such as those based on activated carbon (AC). AC is a metal-free amorphous solid material, easy to obtain from organic matter. However, this material is often used in powder form or as particles, being difficult its regeneration and reuse.

Graphitic carbon nitride (g-C_3N_4) is a polymeric material of metal-free nature, insoluble in water, with proven self-immobilisation capacity onto alumina-silica macrostructures and well-known for its high catalytic activity. In the present work, the synthesis of AC functionalised with different loads of urea (U, a precursor for g-C_3N_4) onto the surface of three-dimensional alumina structures was carried out to avoid the limitations of using AC in powder form. Moreover, this strategy allows the regeneration of the spent AC-based adsorbents by taking advantage of the catalytic performance of g-C_3N_4. The functionalised AC composites were used for venlafaxine (VFX) adsorption in batch and continuous flow operation to verify the adsorption capacity of each material and define the best AC/U ratio for efficient adsorption and catalytic-driven regeneration.

This study revealed that the AC/U ratio that provides a higher adsorption capacity is 50 g_U/g_{AC}. This immobilised composite was tested in continuous flow mode in two different matrices: ultrapure water and drinking water obtained from tap, achieving VFX removals higher than 65% in steady state. Considering the possible regeneration, catalytic wet peroxide oxidation (CWPO) experiments were also conducted, with the functionalised AC composites showing a good performance.

Keywords: adsorption; three-dimensional structures; adsorbent regeneration; activated carbon; graphitic carbon nitride; organic micropollutant.

Resumo

O desenvolvimento e a otimização de tecnologias para o tratamento de águas são cada vez mais necessários devido aos níveis cada vez mais elevados de micropoluentes orgânicos encontrados em matrizes de águas, incluindo água de consumo humano. A adsorção é um dos processos de tratamento mais simples que podem ser aplicados para remover micropoluentes da água e vários adsorventes têm sido desenvolvidos, como os que são à base de carvão ativado (CA). O CA é um material sólido amorfo, livre de metais, fácil de obter da matéria orgânica. Contudo, é comummente usado em pó ou partículas, tornando difícil a sua regeneração e reutilização.

O nitreto de carbono grafítico (g-C_3N_4) conhecido pela sua elevada atividade catalítica, é um material polimérico de natureza livre de iões insolúvel em água com capacidade de auto-imobilização em macroestruturas de sílica-alumina. No presente trabalho foi realizada a síntese de matérias de CA funcionalizados com diferentes cargas de ureia (U, precursor de g-C_3N_4) na superfície de estruturas tridimensionais de alumina, de forma a evitar as limitações da utilização do material na forma de pó. Este processo foi também realizado para facilitar a regeneração dos adsorventes usados tendo como objetivo aproveitar as propriedades catalíticas do g-C_3N_4. Os compósitos funcionalizados de CA foram utilizados em experiências de adsorção de venlafaxina (VFX) em modo contínuo e descontínuo, para verificar a capacidade de adsorção de cada um e descobrir a melhor relação CA/U que possibilite uma adequada adsorção e regeneração catalítica.

O estudo revelou que a relação CA/U que permite uma maior adsorção é 50 g_U/g_{CA}. O compósito imobilizado que foi obtido com este rácio foi testado em modo contínuo com duas matrizes diferentes: água ultrapura e água potável, alcançando remoções superiores a 65% em estado estacionário. Considerando uma possível regeneração, ensaios de oxidação catalítica com peróxido de hidrogénio foram feitos com os compósitos funcionalizados de CA, que demonstraram uma boa performance.

Palavras-chaves: adsorção; estrutura tridimensional; regeneração de adsorvente; carvão ativado; nitreto de carbono grafítico; micropoluente orgânico.

Declaration

I hereby declare, under word of honour, that this work is original and that all non-original contributions is indicated and due reference is given to the author and source.

Porto, 1 July 2024
Joana J. M. Dale

Index

List of Figures

List of Tables

Notation and Glossary

C	Concentration	ppm
C_e	Concentration at equilibrium	ppm
E	Adsorption energy of adsorbent	$kJ \cdot mol^{-1}$
Q	Adsorption capacity	$mg \cdot g^{-1}$
q_e	Adsorption capacity at equilibrium	$mg \cdot g^{-1}$
q_m	Maximum adsorption capacity	$mg \cdot g^{-1}$
t	Time	min
T	Temperature	K or ºC
S_{BET}	Specific surface area by BET method	$m^2 \cdot g^{-1}$

Materials nomenclature

$AC_{commercial}$	Commercial activated carbon (powder)
AC_{MW}	Microwave-treated activated carbon (powder)
AC/U_x	Powdered activated carbon-derived adsorbents (powder)
ACS/U_x	Immobilised activated carbon-derived adsorbents
Bare spheres	Alumina spheres (without carbon materials)
U	Urea

List of Acronyms

3D	Three Dimensional
AC	Activated carbon
AF	Alumina foam
AOP	Advanced oxidation process
BET	Brunauer-Emmett-Teller
CWPO	Catalytic Wet Peroxide Oxidation
DRUV-Vis	Diffuse reflectance ultraviolet-visible (spectroscopy)
EDXS	Energy-dispersive X-ray spectra
FTIR	Fourier transform infrared (spectroscopy)
GCN	Graphitic carbon nitride
HPLC	High-performance liquid chromatography
PFO	Pseudo-first order
PL	Photoluminescence
PPC	Personal care product
PSO	Pseudo-second order
PTFE	Polytetrafluoroethylene
PZC	Point of zero charge
RhB	Rhodamine B
SEM	Scanning electron microscopy
SSNRI	Selective serotonin and norepinephrine reuptake inhibitor
UP	Ultrapure
UV-Vis	Ultraviolet-visible
VFX	Venlafaxine
WWTPs	Wastewater treatment plants

1. Introduction

The biggest reservoirs of water on the planet are the oceans (corresponding to around 97%), so the world population depends on the 3% of available freshwater. The latter is mostly found in glaciers, groundwater and swamps. Other, more easily accessible, freshwater reservoirs like lakes and rivers play a crucial role as industrial, irrigation and drinking water sources [1].

Water contamination occurs when harmful chemicals or microorganisms from human activities are introduced into a water reservoir, degrading water quality and turning it toxic to humans or the environment [2]. The modern world has some challenges due to intense environmental contamination by various organic compounds and consequently, the necessity for development of convenient techniques for their removal. Over the last few years, pharmaceutically active compounds have increased in urban, domestic, industrial, and hospital waters and wastes. Even at low concentrations, their presence is deteriorating the quality of the air, water, and soil [3].

Pharmaceuticals are chemical substances used to prevent, treat, and cure diseases, or to restore, correct, or modify organic functions. In recent years, the use of pharmaceuticals has increased, some were mostly used due to the outbreak of the coronavirus. They belong to the class of contaminants of emerging concern (CECs) and are released to the environment from different sources: domestic (including urine and faeces); improper disposal of sewage by the pharmaceutical industry; medical wastewater discharge, and so forth [4]. They are slightly soluble and highly mobile in water portraying a big problem that demands further attention [3]. Conventional secondary wastewater treatment in wastewater treatment plants (WWTPs), such as activated sludge processes, are not able to remove efficiently these substances, so they are uncontrollably discharged and reach water bodies. As reported in some studies, drinking water treatment processes, such as chlorination and chemical coagulation-sedimentation, are not efficient in the removal of pharmaceuticals, allowing some organic pollutants to remain in the treated water [4, 5]. The pharmaceuticals occurrence in drinking water can cause risks to human health due to long-time exposure [6].

1.1. Framing and presentation of the work

Among various pharmaceutical contaminants, venlafaxine (1-[2-(dimethylamino)-1-(4-methoxyphenyl)-ethyl]-cyclohexan-1-ol; VFX) was chosen as the model pollutant to be removed from water in this work [7]. VFX is an antidepressant that belongs to the class of selective serotonin and norepinephrine reuptake inhibitors (SSNRIs) and is widely used to treat and manage symptoms of depression, cataplexy and social anxiety disorder [8]. Its occurrence in water bodies and drinking water induces several adverse effects such as changes in swimming patterns and stress response mechanisms [9]. Similar to other

pharmaceuticals, VFX is not efficiently removed by conventional wastewater and drinking water treatment plants. Therefore, several technologies have been studied for more efficient removals of this pharmaceutical from water, such as adsorption [10, 11], advanced oxidation processes - AOPs [12], biological technologies [8], electrochemical approaches [13], membrane filtration [14], among others. To select the best-performing technology to implement in wastewater and drinking water treatment, some points must be considered: cost, difficulty of operation and implementation, efficiency and overall sustainability [15].

Adsorption is a surface process that occurs between two different phases in which a molecule (adsorbate) from a fluid bulk (liquid or gas) is transferred to a solid or liquid surface (adsorbent), forming an interface layer, this layer being expressed by physical or chemical interactions [16]. For water and wastewater treatment, several adsorbents have already been developed by researchers. The most used adsorbents are geopolymers [17-19], clay minerals [20], activated carbons [21], metal-organic frameworks [22], zeolites [23], nanosized metal oxides [24] and graphitic carbon nitride [25].

In particular, activated carbon (AC) is a carbonaceous metal-free amorphous solid easily obtained from organic matter, with an extraordinarily large internal surface area and pore volume, that makes it a great adsorbent in many different liquid and gas phase applications [26]. However, because it is mostly used in powder form, its regeneration is difficult and expensive making the reusability process a challenge [27].

Graphitic carbon nitride (g-C_3N_4 or GCN) is a polymeric material insoluble in water, that preserves its stability up to 600 ºC, consisting of tri-*s*-triazine or *s*-heptazine units bonded by tertiary or secondary amino groups, showing resistance to weak acids and bases [25]. This material has a metal-free nature and presents high photocatalytic activity under visible-light illumination. Likewise, g-C_3N_4 is typically used in powder form, so it is difficult to remove it from water after its use [28, 29]. Recently, a work from the LSRE-LCM research group revealed how to perform the self-immobilisation of g-C_3N_4 (without AC) onto alumina-silica macrostructures (ceramic foams) to overcome the disadvantage of powdered catalysts [29]. Hence, the synthesis of g-C_3N_4 from urea was carried out for the first time onto the surface of AC on three-dimensional alumina structures in order to: (i) endow the AC materials of a self-immobilisation mechanism removing the need to filter powder from the treated water and (ii) facilitate the subsequent regeneration of the spent AC-based adsorbents by the catalytic action of g-C_3N_4. Furthermore, the urea-modified AC adsorbents were tested using a tap water matrix to simulate more realistic conditions and the prepared 3D structures were used under continuous flow mode operation for future scale-up applications.

1.2. Main objectives

The main objective is to synthesise functionalised AC composites and perform the self-immobilisation onto 3D alumina structures for VFX removal from water. To accomplish this goal, several short-term objectives were defined: 1) assess the adsorption capacity of the modified AC materials by selecting the best proportion of AC and urea (precursor for g-C_3N_4); 2) immobilise the AC-based composites onto macrostructured alumina spheres; 3) investigate the influence of the water matrix on the adsorption mechanism; and 4) employ catalytic wet peroxide oxidation (CWPO) for future regeneration of spent adsorbents.

1.3. Organisation of the dissertation

This dissertation is organised in six chapters. In the present chapter, a brief introduction about the proposed work is presented. Chapter 2 shows the adsorption fundamentals, a literature review of AC and g-C_3N_4 in adsorption of VFX and other pollutants, as well as their use as a catalyst. A description of the materials and methods is made in Chapter 3. Chapter 4 discusses the characterisation results of the functionalised AC composites, the adsorption studies carried out with the composites and the respective catalytic activity. The conclusions and the assessment of the work done are presented in Chapters 5 and 6, respectively.

2. Context and State-of-the-art

2.1. Principles of adsorption

In adsorption, if a liquid material is an adsorbent (liquid-gas or liquid-liquid system), the interfacial layer is called film, micelle, or emulsion. When it is a solid-liquid or solid-gas system, the adsorbent is solid, so the adsorption process mechanism follows an interfacial layer model [16].

The equilibrium existent between the adsorbent and the bulk phase is described by the interfacial layer, explained by two principles: physical and chemical adsorption. Physical adsorption or physisorption leads to no changes of the chemical structure for both adsorbate and adsorbent, and the bonding between them is weak Van der Walls forces. Chemical adsorption or chemisorption occurs when the chemical bonding between adsorbate and adsorbent is an ionic or a covalent bond, by rearrangement of electron density between them [16].

The interaction between the adsorbate and adsorbent can be described by adsorption isotherms, which represent the relation between the amount of adsorbate per unit mass of adsorbent and the adsorbate concentration or pressure in the bulk solution at a constant temperature [16].

The Langmuir isotherm was originally derived from studying the adsorption of gases by solids, is the simplest isotherm model and describes the single adhesion layer on the homogeneous surface, where the attraction between molecules adsorbed on the adsorbate and non-adsorbed analyte in the bulk solution decreases as they are getting away from the adsorbate surface. The Langmuir model is proposed for low concentrations assuming that adsorption is performed in a monolayer with no attraction between molecules on the surface of adsorbate. So, for modelling multi-layer adsorption on heterogeneous surfaces, the Freundlich isotherm was suggested, representing a specific case of the Langmuir model. This isotherm indicates a high affinity of the adsorbate for the adsorbent, suggesting chemisorption, and occuring when adsorbate-adsorbent interaction is stronger than adsorbate-solution interaction. Another model used to describe adsorption is the Dubinin-Radushkevich (D-R) isotherm, which is similar to the Langmuir isotherm but rejects the homogeneous surface. In this isotherm, the adsorption mechanism is done by pore-filling of adsorbent rather than layer-by-layer adsorbent surface coverage [16]. In addition, Sips isotherm, also known as Langmuir-Freundlich model, is the adsorption model that describes the adsorption mechanism as a combination of diffusion at low solute concentrations and monolayer formation at high solute concentrations [30].

2.2. Adsorbent synthesis and modification

AC is a type of porous carbon obtained by carbonisation of carbonaceous materials with dehydrating chemicals or by treatment of a char with oxidising gases. These carbons exhibit a high surface area and a high degree of porosity.

Known as the oldest adsorbent in water purification and the predecessor of modern AC, charcoal had its specific adsorptive properties first discovered by Scheele for the treatment of gases in 1773, followed by solutions decolourisation in 1786, allowing him to provide the first systematic account of the adsorptive power of charcoal in the liquid phase [31]. The commercial production of porous carbon dates to the beginning of the 20th century, being produced from wood and peat. The need for protective gas masks during World War I boosted the development of granular AC (GAC) from coconut shells; thereafter the applications of AC were extended to the purification of drinking water [32].

In adsorption processes, AC plays a crucial role in the removal of impurities from gases and liquids. The surface of AC causes a higher concentration of adsorbate at the interface than in the bulk fluid due to physical forces (Van Der Walls type) that bind the molecules from the liquid or gas phases [32]. Chemisorption may occur on active sites of the carbon surface as consequence of stronger valence forces. Therefore, the adsorption capacity of AC depends on its physical (including specific surface area, pore volume and pore structure, among others), and surface chemical properties (surface acidity and alkalinity, functional groups and electrochemical properties), consequently, the latest research on AC has been focused on the modification and characterisation of the material in order to meet the growing demand for cleaner air and water [32, 33].

In the AC structure can be present atoms such as oxygen, hydrogen, sulphur and nitrogen as functional groups chemically bonded to the structure. These groups can play a role in the adsorption capacity of AC and are mainly derived from activation processes [34], precursors [35], thermal treatment and post-chemical treatment [31, 36].

Several methods were reported in the literature for modification of AC structure. For instance, Salas *et al*. [30] prepared a novel adsorbent doping AC with whey protein fibrils (WPF). The AC/WPF membrane exhibited good specific surface area (456 $m^2\ g^{-1}$), porous structure and prominent functional groups (amide and amine groups from whey proteins and hydroxyl groups of AC) to capture arsenate resulting an adsorption capacity of 0.15 mmol g^{-1} at 30 ºC.

Wei *et al*. [37] prepared a metal-free catalyst based on g-C_3N_4 supported on AC through an *in situ* thermal approach for degradation of pollutants in the presence of peroxymonosulfate (PMS) without light irradiation. This study showed that g-C_3N_4 supported on AC catalyst exhibited an unprecedented high performance for degradation of organic pollutants in the presence of PMS with an acid orange 7 dye removal of 96.4 % achieved within 10 min. It also

demonstrated that the adsorption ability of the g-C_3N_4/AC catalysts decreased for high g-C_3N_4 loadings, with 5.2% proving to be the best-performing loading for adsorption.

More recently, in the nineteenth century, Liebig was responsible for the first description of the synthesis of graphitic carbon nitride-based material, converting melamine into a melon-like analogue of g-C_3N_4 [25]. Nowadays, g-C_3N_4 synthesis is performed mostly via thermolysis methods with inexpensive earth-abundant precursors, such as cyanamide, urea, thiourea, dicyandiamide, cyanamide, and melamine [28]. Among the possible g-C_3N_4 precursors, urea showed the best performance concerning the production of g-C_3N_4 with high photocatalytic activity [38].

In a previous work, Chávez *et al*. prepared a g-C_3N_4 that is self-immobilised onto microporous and reticulated ceramic alumina/silica foams (AF) by a facile one-pot and *in-situ* method by urea polymerisation directly onto ceramic foams [29], using a method adapted from elsewhere [39]. This heating program yields a 5% weight yield of urea/g-C_3N_4, after attempting different concentrations of urea with fresh AF. To remove non-polymerised material and non-adhered g-C_3N_4, the g-C_3N_4/AF samples obtained were washed with ultrapure (UP) water and sonicated for 5 min. To complete the procedure, the samples were blasted with compressed air, immersed in boiling UP water, and dried at 100 ºC. Powdered g-C_3N_4 was also prepared by thermal condensation of the solid urea reagent with the same thermal treatment [29].

2.3. AC and g-C_3N_4 in adsorption

The data from **Figure 1** were retrieved from the Scopus® database. **Figure 1** shows the evolution of the number of documents published over the years, since 2010, where the expressions “carbon nitride” or “graphitic carbon nitride” or “C_3N_4” and “activated carbon” or “AC” were found in the article title, keywords, or abstract. It is clear the difference between the number of publications related to each material, more documents being found for AC, as expected. The database showed a total of more than 32 000 results for “carbon nitride” or “graphitic carbon nitride” or “C_3N_4”, and above 417 000 results for “activated carbon” or “AC”. From the results of carbon nitride materials, the database showed 543 results for adsorption, most of them being related to the adsorption of dyes and metals; while for activated carbon there were already more than 30 000 results related to adsorption.

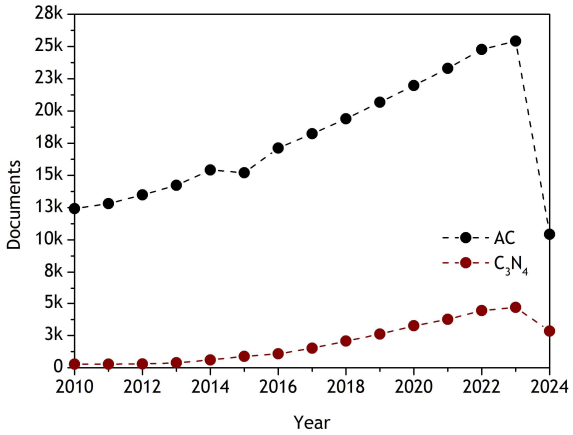

Figure 1. Number of publications by year regarding the use of AC or g-C_3N_4. Source: Scopus® database, June 2024. Keywords: "carbon nitride", "graphitic carbon nitride", "C_3N_4", "activated carbon" and "AC".

When used as adsorbents, AC, g-C_3N_4 and their composites interact with the adsorbate following several mechanisms, such as electrostatic interaction, π-π interaction, hydrogen bonding, complexation, and cation bridge [25].

- **Electrostatic interaction:** Occurs when both adsorbent and pollutant have electric charges. Usually, the electrostatic interaction depends on the surface charge of the adsorbent and pollutant and is the most common mechanism route for the adsorption of dyes on the g-C_3N_4 surface [40]. For adsorptive removal of different dyes under UV and visible light, Zhang *et al*. synthesised a composite based on ZnO-layered double hydroxide and g-C_3N_4 and observed that electrostatic and π-π interaction were two synergetic steps in the adsorption process [41].
- **π-π interaction:** When aromatic pendant groups are present in the adsorbent and pollutant structure. This interaction occurs between two aromatic groups via non-covalent bonds [40]. Haydar et al. concluded that *p*-nitrophenol adsorption mechanism onto activated carbon, prepared from olive stones modified through oxidation by nitric acid or sodium hypochlorite, occurred *via* π-π interaction [42]. A carbon-doped g-C_3N_4 was used to remove methylene blue from an aqueous solution by Ren *et al*. and in this case the adsorption process was physical and mainly *via* both π-π and electrostatic interactions [43].
- **Hydrogen interaction:** A type of electrostatic interaction that involves hydrogen ions (H^+) and occurs when proton donor and acceptor groups of the process are present [40]. Nazar *et al*. found that the key mechanism of methylparaben (MP) adsorption onto Calgon Carbon (Filtrasorb-400) was via hydrogen interaction between the –OH functional groups of MP molecules [44]. This hydrogen bonding can take place between g-C_3N_4 composites and pollutant molecules [45]. Zhao *et al*. suggested that

during malachite green adsorption by a g-C_3N_4/Fe_3O_4/zeolite nanocomposite there might be hydrogen binding interactions, since both g-C_3N_4 and the dye contain nitrogen atoms [46].

- **Complexation:** Occurs with metal-based adsorbent composites. These composites have metal ligands that cause multi-atom formation through adsorption. A g-C_3N_4/$MnFe_2O_4$/iron-metal organic framework composite was fabricated by Wang *et al*. to adsorb personal care products (PPCPs) from aqueous solution; the results showed that the prepared material could adsorb the molecules by a complexation mechanism [40, 47]. AC was doped with Mg and Al for adsorption of SO_4^{2-} in groundwater by Abushawish *et al.*, who found through material characterisation that the main mechanism in SO_4^{2-} adsorption was surface complexation [48].
- **Cation bridge:** When there is a possibility of exchange between ionised cation of the charged pollutant and charged metal compounds in g-C_3N_4 composite structures. Wan *et al*. synthesised a novel protonated g-C_3N_4 and acid-activated montmorillonite composite to adsorb phosphate anions and lead (II) from aqueous media; according to the results, the main adsorption mechanism was related to cation bridge [40, 49].

Searching for “carbon nitride” or “graphitic carbon nitride” including “activated carbon” on Scopus® database, 279 publications were found. From those, 15 were related to the adsorption of organic pollutants in the liquid phase with a powdered material. Pei *et al*. synthesised a g-C_3N_4/AC composite *via* ultrasonic irradiation to remove fluoride from water by adsorption. The synthesised composite had higher fluoride removal capacity of 92.7 mg g^{-1} compared to 2.1 mg g^{-1} for bare AC. The composite achieved up to 90% defluoridation of a real wastewater containing 8.7-12 mg L^{-1} of fluoride and a Langmuir isotherm model was fitted to the data obtained in batch conditions [50]. The regeneration-adsorption cycle was repeated for five cycles and it was observed that the fluoride removal efficiency decreased from 91% in fresh to 87% after 4 regeneration cycles [50].

Due to its possible excitation under near-visible light irradiation and exceptional charge transfer abilities, g-C_3N_4 has been used as a heterogeneous catalyst in photoelectrochemical degradation of organic pollutants in water [51]. Torres-Pinto *et al*. used a g-C_3N_4 particle electrode to remove some pharmaceuticals (diclofenac, ibuprofen, and fluoxetine) from water by photoelectrocatalytic (PEC) treatment; due to photo-responsive and semiconducting properties of g-C_3N_4. Authors concluded that PEC degradation of diclofenac was more effective comparing with photocatalytic and electrocatalytic processes alone. In their study, g-C_3N_4 showed a remarkable durability and promising potential for PEC applications, and in particular for degradation of pharmaceuticals [51].

Moreover, g-C_3N_4 can activate other oxidants such as peroxymonosulfate (PMS) [52], peroxydisulfate (PDS) [53, 54], hydrogen peroxide (H_2O_2) [55], ozone (O_3) [56] and free chlorine species ($HOCl/ClO^-$) [57].

Kim *et al.* conducted a study in which PMS was activated by AC to degrade urea [58]. The AC exhibited various surface oxygen functional groups (C–OH, C=O and C–O) which enhanced its catalytic activity. The same principle was defended by Tan *et al.*, who synthesised an integrated activator and catalyst by vacuum ball milling of PS and AC [59].

2.4. Adsorbent regeneration

Regeneration can be described as a retrieval process of spent adsorbents for reuse, with basis on economical and sustainable reasons. The optimal regeneration method will focus on the retrieval of the adsorbents without destroying them [60]. This process can be repeated several times, but the regenerated adsorbent often exhibits reduced adsorption capacity [61]. There are several techniques to recover and regenerate adsorbents, such as filtration [62], microwave irradiation [63], magnetic separation [64], thermal desorption [65], supercritical fluid regeneration [66], solvent regeneration [67], AOPs [68, 69], and microbial-assisted adsorbent regeneration [70].

AOP-based systems have gained attention in water treatment owing to their effectiveness for the oxidation of recalcitrant organic molecules [71], such as CWPO, ozonation or using other oxidising agents integrated or not with catalytic processes activated by electrical power sources or external ultraviolet (UV)/visible radiation. In particular, CWPO is a low-cost technology in which the organic pollutants are degraded by hydroxyl radicals ($HO^{\bullet}$) generated from partial decomposition of H_2O_2 promoted by an appropriate catalyst [72].

2.5. Adsorption of venlafaxine

Several studies were attempted for VFX removal by means of AOPs [12, 73], photocatalysis [74, 75], or adsorption [76, 77]. VFX can be adsorbed even by polypropylene microplastics (PP MPs) in fresh and seawater via electrostatic interaction. For instance, the study made by Xu *et al.* demonstrated that PP MPs have a strong adsorption capacity for VFX and chemisorption was identified as the primary mode using Dubinin-Radushkevich model [11]. Jaria *et al.* carried out a study with sludge based-AC functionalised structures for adsorption of six pharmaceuticals, namely VFX, carbamazepine (CBZ), lorazepam (LOR), sulfamethoxazole (SMX), piroxicam (PIR) and paroxetine (PAR). The study revealed that the functionalised AC structure with amine functional groups (AC-NH_2) shows a great specificity for VFX [78]. Regarding studies of g-C_3N_4 for VFX removal, there were no studies found using g-C_3N_4 specifically as an adsorbent, only as a photocatalyst.

3. Materials and Methods

3.1. Reagents

Powdered activated carbon (Norit w35) was obtained from CABOT Corporation. Urea (NH_2CONH_2, 99.8%) was obtained from VWR CHEMICALS. Aluminium oxide (Al_2O_3 α-phase, catalyst support, low surface area, trimodal) was supplied by Thermo Scientific Chemicals. Venlafaxine hydrochloride ($C_{17}H_{27}NO_2HCl$, >98.0%) was obtained from Tokyo Chemical Industry Co., LTD. Rhodamine B ($C_{28}H_{31}ClN_2O_3$, ~95%) was obtained from Sigma® Life Science. Ultrapure (UP) water was produced in a Direct-Q Millipore system (Merck Millipore, Billerica, MA, USA).

3.2. Preparation of adsorbents

Figure 2 shows a general scheme of the synthesis procedure of the adsorbent, while **Figure 3** depicts photographs of the prepared materials.

Powder adsorbents – AC/U_x

500 mg of commercial AC ($AC_{commercial}$) and different dosages of urea (5, 20, 25, 30, 50 and 100 g) were poured in 50 mL of UP water to obtain AC/U_x powdered composites (*x* being the urea load) via thermal decomposition. Each mixture of AC and urea in water was firstly stirred to dissolve the urea and then heated to vaporise the excess of water, obtaining a slurry that was placed in a crucible that was placed inside a microwave furnace, under static air atmosphere. The microwave was programmed to heat at 2 ºC min^{-1} until 450 ºC during 2 h, followed by a ramp heating until 550 ºC, keeping this temperature for 4 h (i.e. a total of 6 h inside the microwave). Afterwards, the synthesised material was washed several times with distilled water and dried overnight, yielding the powder adsorbents labelled as AC/U_x (*x* = 5, 20, 25, 30, 50 or 100). Pristine AC ($AC_{commercial}$) underwent the same treatment procedure without the addition of urea, leading to AC_{MW}.

Self-immobilised 3D adsorbents – ACS/U_x

A similar procedure was performed for the self-immobilisation of AC/U onto the 3D support, differing by the addition of Al_2O_3 spheres onto the crucible along with the prepared slurries (**Figure 2**). Before use, the commercial alumina spheres were boiled in water, rinsed and dried before addition into the aqueous solutions of 500 mg of commercial AC with different dosages of urea and then transferred to the crucibles. After the abovementioned thermal treatment, the obtained functionalised spheres were thoroughly rinsed with distilled water and sonicated for 1 h in an ultrasonic cleaner to remove any loose powder at the surface of the spheres.

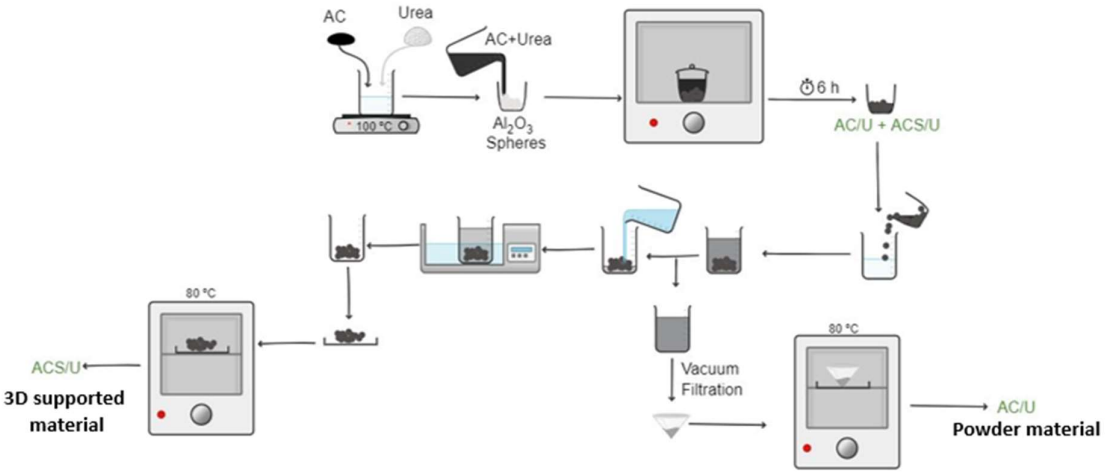

Figure 2. Schematic representation of the synthesis of the prepared adsorbents.

Figure 3 shows the adsorbents obtained which were named as AC/U_x for powders and ACS/U_x for the immobilised materials, where *x* represents the urea load.

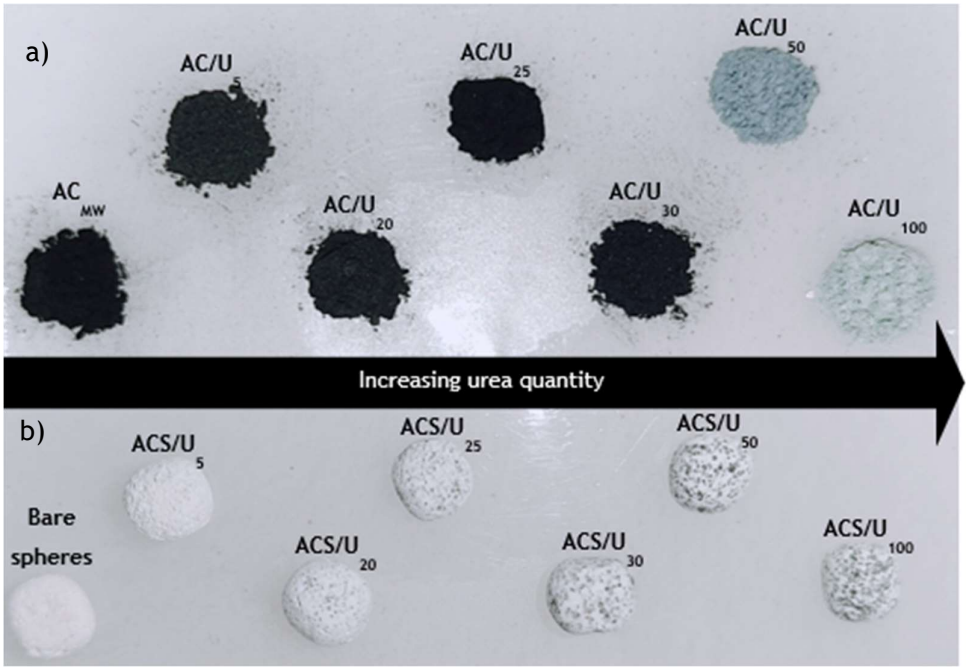

Figure 3. Photographs of functionalised AC composites: **a)** AC/U_x and **b)** ACS/U_x.

3.3. Adsorbents characterisation

3.3.1. Diffuse reflectance ultraviolet-visible spectroscopy

The optical properties of the adsorbents were determined by diffuse reflectance ultraviolet-visible spectroscopy (DRUV-Vis) in a JASCO-V560 spectrometer with an integrating sphere attachment (JASCO ISV-469). The spectra obtained were recorded in diffuse reflectance mode at a wavelength range of 220 to 800 nm.

3.3.2. Fourier Transform Infrared Spectroscopy

The FTIR Fourier transform infrared spectroscopy (FTIR) measurements were performed in a JASCO FT/IR-6800 spectrometer (JASCO Analytical Instruments) equipped with a MIRacle™ Single Reflection (Attenuated Total Reflectance ZnSe crystal plate) from PIKE Technologies.

3.3.3. Photoluminescence (PL) spectroscopy

The emission spectra of the adsorbents were recorded on a JASCO (FP-82000) spectrofluorometer after excitation at 370 nm, with the emission recorded from 390 to 800 nm.

3.3.4. Point of zero charge

For each selected adsorbent, 15 mg of material were added to 10 mL with UP water at different pH values, previously adjusted with HCl and NaOH, considering a pH range from 2 to 10. The dispersions were left during 24 h in dark conditions. The point of zero charge (PZC) was determined from the interception of the final pH *vs.* initial pH plot with a diagonal line.

3.3.5. Scanning electron microscopy

Scanning electron microscopy (SEM) was used to examinate and analyse the microstructure morphology and chemical composition of the adsorbents using a JEOL JSM-840 instrument with an Oxford Inca Energy Si(Li) detector for energy-dispersive X-ray spectroscopy (EDXS).

3.3.6. Specific surface area and pore volume

The specific surface area was determined by the Brunauer-Emmett-Teller method (S_{BET}) and the pore volume by the Barret-Joyner-Halenda method. These analyses were carried out in a Quantachrome Autosorb iQ automated gas sorption analyser apparatus by multipoint analysis of N_2 adsorption-desorption isotherms at -196 ºC. The samples were previously degassed at 120 ºC and under vacuum for 5 h.

3.4. Adsorption experiments

Powder adsorbents

Different loads of commercial AC (0.05, 0.10, 0.25, 0.30 $g \cdot L^{-1}$) were tested in a batch reactor containing 50 mL of 5 ppm VFX. The aqueous solutions were stirred for 60 min at 700 rpm, and samples were withdrawn periodically and filtered with a hydrophilic PTFE filter (13 mm,

0.22 μm), as shown in **Figure 4**. Powdered AC/U_x adsorbents were tested with a specific load of 0.10 $g \cdot L^{-1}$.

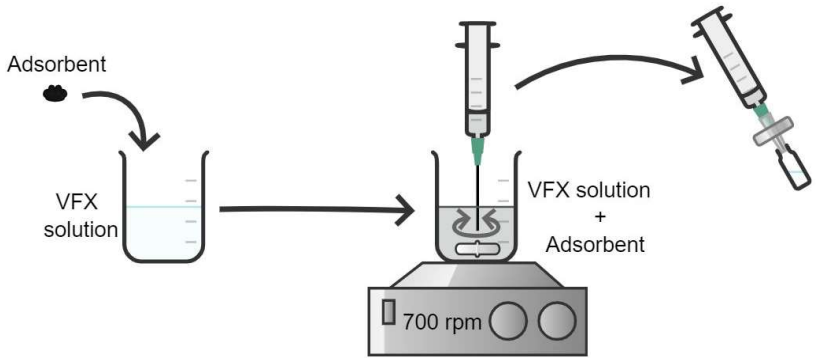

Figure 4. VFX adsorption in batch operation mode.

Self-immobilised 3D adsorbents

Immobilised ACS/U_x adsorbents were placed in a continuous flow mode cell with a total length of 5 cm and inner diameter of 1.6 cm (**Figure 5**). The cell, containing the spheres, was connected to a peristaltic pump with flow rate of 0.22 $cm^3 \cdot min^{-1}$. Each experiment was carried out with a constant inlet of 5 ppm of pollutant solution during 2 h, taking samples periodically at both the inlet and outlet.

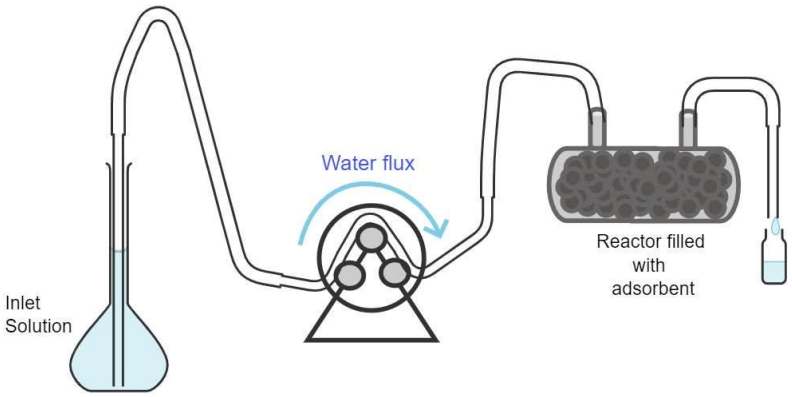

Figure 5. VFX adsorption in continuous flow operation mode (packed-bed configuration).

3.4.1. Adsorbent regeneration

CWPO was studied to regenerate the synthesised adsorbents (powder and immobilised ones). The CWPO tests were carried out following the same scheme as in adsorption within 60 min (batch) and 2 h (plug flow) of experiment with 2.5 mM H_2O_2 concentration. In batch experiments, H_2O_2 was added to the reactor and stirred at 700 rpm for 60 minutes. In the continuous flow reactor, H_2O_2 was added to the inlet solution. Samples were withdrawn periodically for pharmaceutical and H_2O_2 quantification.

3.5. Analytical methods

3.5.1. Ultraviolet-visible spectroscopy

The RhB concentration was measured by absorbance via ultraviolet-visible (UV-Vis) spectroscopy in a JASCO-V560 UV-Vis spectrophotometer, with a double monochromator and a double-beam optical system. The absorbance values were recorded at a wavelength of 554 nm.

3.5.2. High-performance liquid chromatography

The samples collected during the adsorption and regeneration experiments were analysed by high-performance liquid chromatography (HPLC) using a Shimadzu© instrument equipped with a photodiode array detector (SPD-M20A) and a Fluorescence detector (RF-20A xs), an autosampler (SIL-30C), a solvent delivery pump (LC-30AD) at a flow rate of 0.2500 mL min^{-1}, a column oven (CTO-40C) with a Kinetex™ XB-C18 100 Å column (100 mm x 2.1 mm, 1.7 µm particle diameter) supplied by Phenomenex Inc. at 30 ºC.

For VFX concentration analysis, the HPLC method consisted in isocratic elution of water (A): acetonitrile (B) (77:23) for 5 min, and an excitation and emission wavelength of 230 nm and 300 nm, respectively.

3.5.3. H_2O_2 concentration

The determination of consumed H_2O_2 during CWPO was performed in a quartz cuvette after mixing 300 µL of sample, 300 µL of sulphuric acid (0.5 M) and 30 µL of titanium oxysulphate. The absorbance was read at 405 nm in a JASCO V-560 UV-Vis spectrophotometer.

3.6. Adsorption kinetics

Adsorption kinetics can be expressed by pseudo-first (PFO) and second (PSO) order models presented in **Table 1** [79].

Table 1. Adsorption kinetic models used for VFX and RhB adsorption analysis.

Model	Equation	Parameters
Pseudo-first order	$q = q_e(1 - \exp(-k_1 t))$	q = adsorption capacity ($mg \cdot g^{-1}$) q_e = adsorption capacity at equilibrium ($mg \cdot g^{-1}$) k_1 = PFO rate constant (min^{-1})
Pseudo-second order	$t/q = \frac{1}{k_2 q_e^2} + \frac{1}{q_e t}$	k_2 = PSO rate constant ($g \cdot mg^{-1} \cdot min^{-1}$)

3.7. Adsorption isotherms

The equations used in the study of adsorption isotherms were Langmuir, Freundlich, Sips and D-R in linearised form (**Table 2**).

Table 2. Adsorption isotherm models used in VFX and RhB adsorption analyses.

Model	Equation	Parameters
Langmuir	$q_e = q_m K_L \frac{C_e}{1+K_L C_e}$	q_m = maximum adsorption capacity ($mg \cdot g^{-1}$) K_L = Langmuir constant ($L \cdot mg^{-1}$)
Freundlich	$q_e = K_F C_e^{1/n}$	K_F = Freundlich constant ($mg \cdot g^{-1}$) n = adsorption intensity
Sips	$q_e = q_m K_S \frac{C_e^{\beta_S}}{1+K_S C_e^{\beta_S}}$	q_m = maximum adsorption capacity ($mg \cdot g^{-1}$) K_S = Sips constant ($L \cdot mg^{-1}$) β_S = heterogeneity
D-R	$q_e = q_m \exp\left(-K_{DR}(RT\ln\left(1+\frac{1}{C_e}\right))^2\right)$ $E = (2\ K_{DR})^{-0.5}$	q_m = theoretical adsorption capacity ($mg \cdot g^{-1}$) K_{DR} = D-R constant ($mol^2\ kJ^{-2}$) R = universal gas constant (8.31 J mol^{-1} K^{-1}) T = absolute temperature (K) E = Adsorption energy of adsorbent ($kJ \cdot mol^{-1}$)

4. Results and Discussion

4.1. Adsorbents characterisation

4.1.1. DRUV-Vis

Figure 6 shows the DRUV-Vis spectra of AC-derived adsorbents, and pristine g-C_3N_4. The AC commercially obtained and treated in MW show very similar spectra, keeping almost a constant complete absorbance in the studied range. The spectrum of bare g-C_3N_4 is typical of this material: *i.e.*, maximum absorbance below 390 nm, above which absorbance decreases with a strong slope to 550 nm. The AC/U_5, AC/U_{20} and AC/U_{25} materials do not show evident characteristic spectra of g-C_3N_4, probably owing to the deep permeation of urea during the functionalisation treatment or to the low amount used. In contrast, AC/U_{100} already presents the representative curve of g-C_3N_4 attributed to the higher amount of urea used during synthesis. In fact, for increasing loads of urea, the spectra shift from AC_{MW} (0% urea, 100% AC) to g-C_3N_4 (100% urea, 0% AC) is observed in the present work.

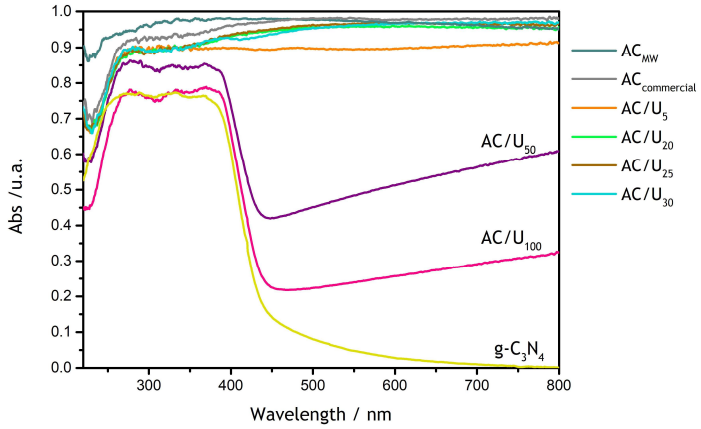

Figure 6. DRUV-Vis spectra of $AC_{commercial}$, AC_{MW}, g-C_3N_4 and the AC/U_x powdered prepared materials.

In the case of immobilised materials, the bare spheres (**Figure 7**) show a singular absorption in the UV range around 250-300 nm, also clear for ACS/U_5, whereas the ACS/U_{25} material presents a maximum absorbance near the peak of bare spheres together with an overall spectrum shape more similar to g-C_3N_4, indicating the formation of g-C_3N_4 on the alumina's surface.

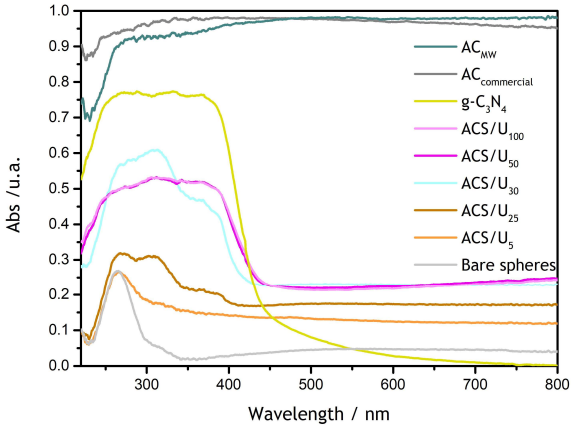

Figure 7. DRUV-Vis spectra of $AC_{commercial}$, AC_{MW}, g-C_3N_4, bare pheres and the immobilised prepared materials.

4.1.2. FTIR Spectroscopy

The FTIR spectra of the composites with higher urea dose, namely AC/U_{50} and AC/U_{100}, have very similar bands to those observed for bare g-C_3N_4 (**Figure 8a**). In the spectrum of g-C_3N_4 is possible to identify 4 distinct regions. The first region identified (1) is a broad band at 3000-3300 cm^{-1} caused by N–H and N–H_2 groups stretching vibrations of primary and secondary amine groups [80] and for O–H stretching vibration modes [81]. The second region (2) contains two bands, at 1622 and 1552 cm^{-1}, corresponding to C=N groups stretching vibrations. The third region (3) has three bands, at 1399, 1316, and 1228 cm^{-1}, originated by C–N stretching vibrations [82, 83], these bands disappear as the urea content decreases; the last one (4) corresponds to the aromatic carbon nitride heterocycle, which bands are at 887 and 804 cm^{-1} [84], with the latter band consistent in all materials.

The spectra of AC (pristine and thermally treated) showed two main regions (5) and (6) (**Figure 8b**). The first one corresponds to a peak of C=O, present in all composites at 1730 cm^{-1}; and the second one is a low intensity band attributed to C–O groups at 1098 cm^{-1}.

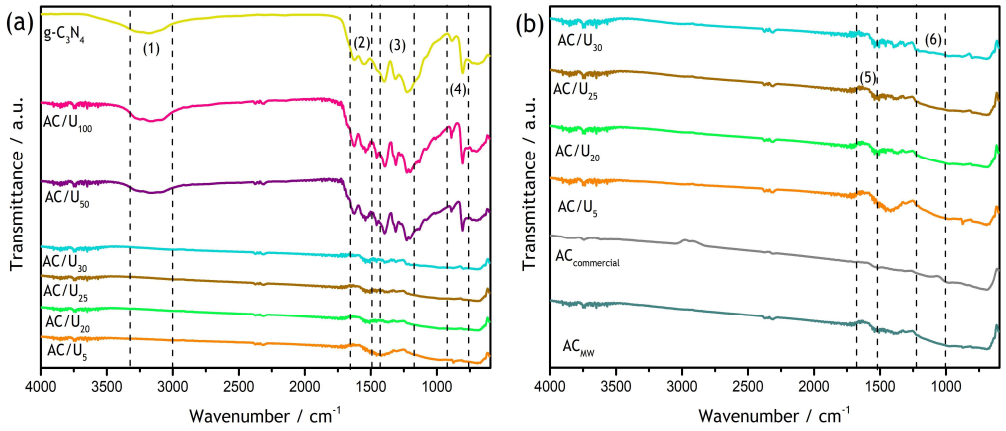

Figure 8. FTIR spectra of **(a)** bare g-C_3N_4, **(b)** pristine and commercial AC materials and **(a,b)** different powdered AC/U_x composites.

ACS/U_{100} (**Figure 9a**) showed a very similar spectrum to its powdered composite (**Figure 8a**) owing to the high surface coverage of the alumina structure. The remaining composites (**Figure 9a**) showed spectra more similar to the bare alumina sphere, with some regions of C–N stretching vibrations and a slight peak from C–O groups at 1098 cm^{-1}, denoting the efficient immobilisation (**Figure 9b**).

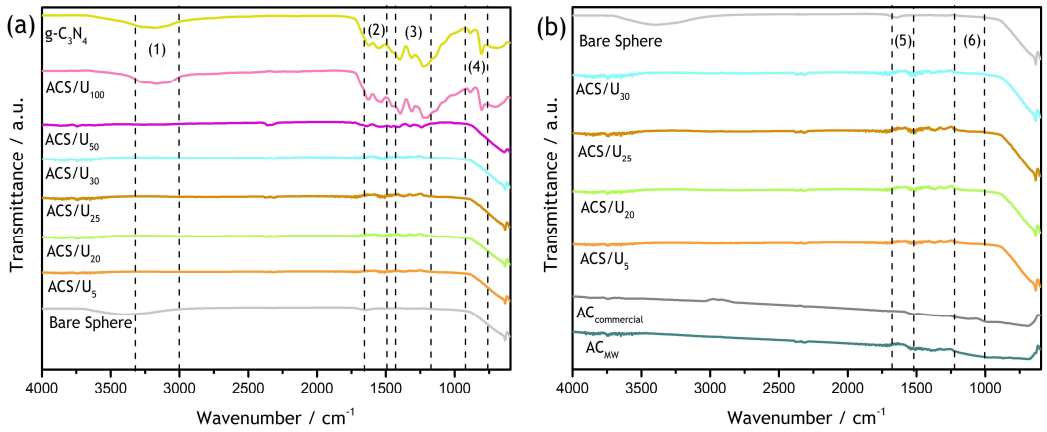

Figure 9. FTIR spectra of **(a)** powder g-C_3N_4 and **(b)** powder AC and comparison with **(a,b)** the self-immobilised ACS/U_x composites and bare alumina spheres.

4.1.3. Photoluminescence emission spectroscopy

g-C_3N_4 and its composites are known as optical semiconductors and their PL emission spectra are typically composed of three Gaussian curves: a strong peak near ~450 nm and two shoulders at higher wavelengths (~490 and ~520) [39]. As it can be seen in **Figure 10a**, the materials with higher urea content showed some photoluminescence due to electronic transitions caused by the functionalisation of AC with urea; thus, the formation of some g-

C_3N_4 is also evident by this characterization technique. However, for lower urea contents, such as AC/U_5 and AC/U_{20}, a low intensity PL emission signal was obtained, very close to bare AC (**Figure 10b**).

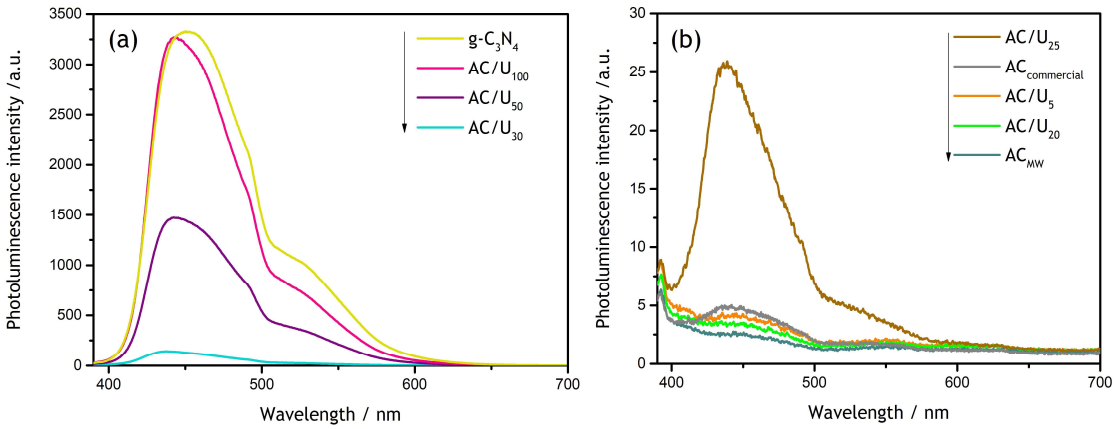

Figure 10. Photoluminescence spectra of powdered **(a)** g-C_3N_4 and AC/U_x (x ≥ 30) and **(b)** bare AC (commercial and MW-treated) and AC/U_x composites (x ≤ 25).

The ACS/U_x spheres with higher content of urea (x≥25, i.e. AC/U_{30}, AC/U_{50} and AC/U_{100}) showed some varying PL emission intensities (**Figure 11a**), that were not as linear as the observed for the powdered materials (**Figure 10a**). This can be eventually explained by the composite unequal distribution on the surface of the spheres. Moreover, the bare alumina spheres are not identical amongst themselves and, therefore, some might allow for easier self-immobilised composites than others.

AC alone shows negligible photoluminescence and Al_2O_3 (bare spheres) a very low signal (**Figure 11b**). Accordingly, the immobilised composites with lower urea content (ACS/U_x, x ≤ 20) showed very low intensities, but between alumina and AC, due to the low addition of AC onto the surface of Al_2O_3 spheres.

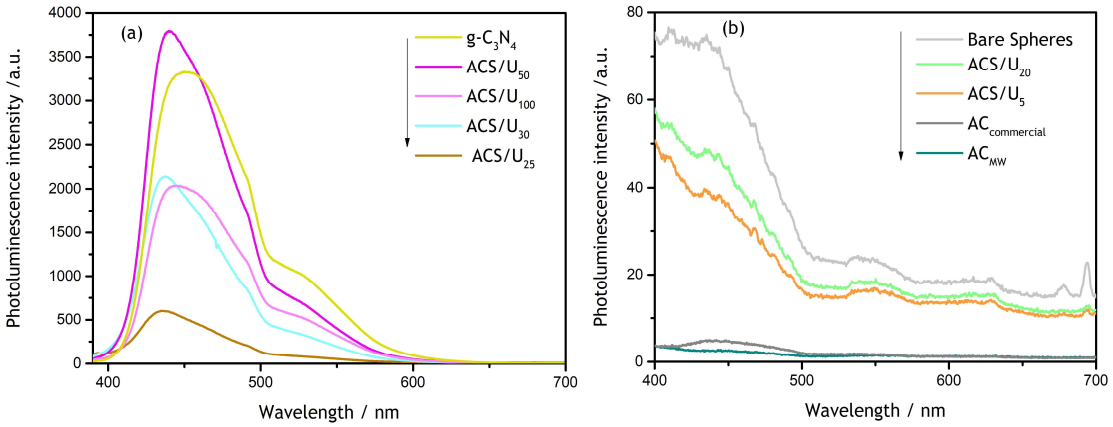

Figure 11. Photoluminescence spectra of **(a)** powder g-C_3N_4 and ACS/U_x spheres ($x \geq 25$) and **(b)** bare spheres, AC (commercial and MW-treated) and ACS/U_x spheres ($x \leq 20$).

4.1.4. Point of zero charge

To understand the surface chemistry and the influence of the pH in materials surface, the point of zero charge (PZC) of selected materials was determined. AC/U_{25} and AC_{MW} showed pH_{PZC} values of 9.2 and 9.4 (**Figure 12c** and **12d, respectively)**. Since AC/U_{25} is mostly constituted of AC, similar pH_{PZC} values were already expected. Under these pH values, the surface of the materials will be positively charged, once the surface anions will attract cations to its surface; for pH higher than these PZC values, the surface will be negatively charged.

Similar pH_{PZC} values were found for ACS/U_{25} and for bare alumina, 7.6 and 7.4 respectively (**Figure 12a** and **12b)**. This means that the surface of these materials is mostly charged negatively for pH values greater than 7.6 and 7.4 respectively, and positively charged for lower pH values. The similarity between their pH_{PZC} values may be due to the fact that the spheres covered with AC composites were crushed for characterisation purposes, meaning there will be a higher alumina content (bulk) than of AC/U_x (surface).

Torres-Pinto *et al*. reported a pH_{PZC} value of 6.9 for g-C_3N_4 obtained by using urea as precursor [38], slightly lower than the pH_{PZC} of AC/U_{25}.

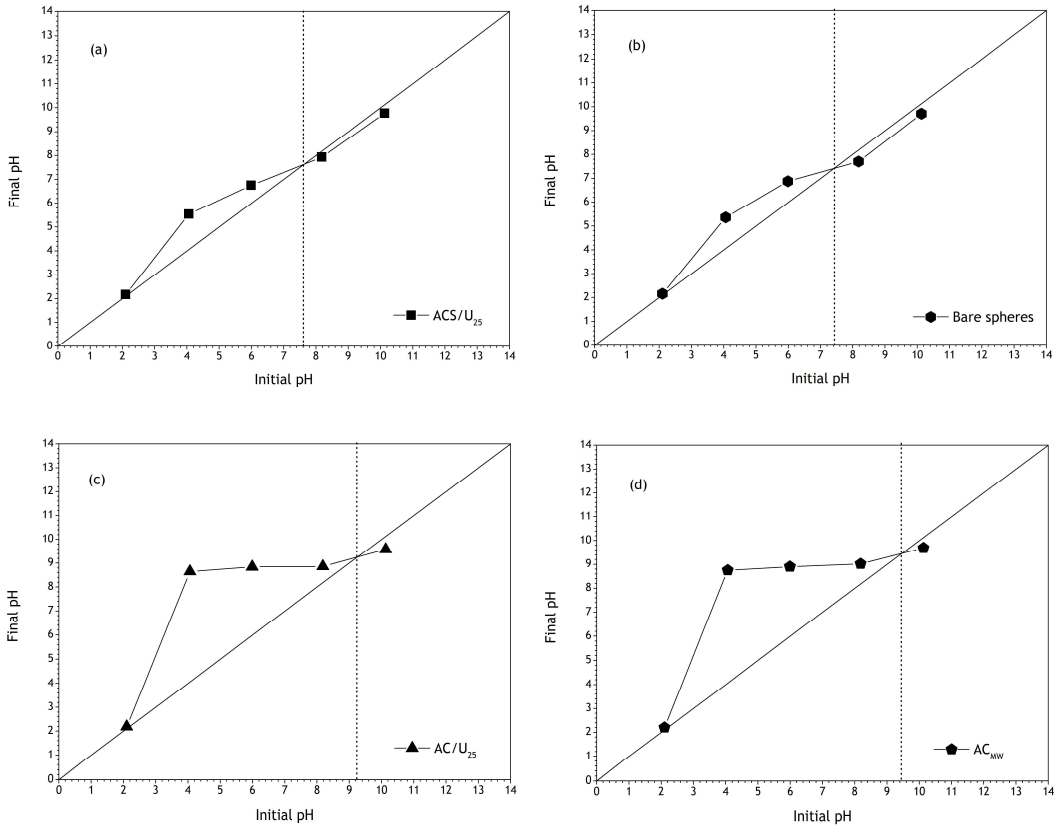

Figure 12. PZC determination of **(a)** ACS/U_{25}, **(b)** bare spheres, **(c)** AC/U_{25} and **(d)** AC_{MW}.

4.1.5. Specific surface area and pore volume

Figure 13 shows the N_2 adsorption-desorption isotherms for the $AC_{commercial}$ and AC/U_{25} powder materials. It is observed that at lower relative pressures, there is indication of the micropore region, and then there is a monolayer formation until slightly higher relative pressures where the multilayer is formed. At higher relative pressures, capillary condensation happens. This type of behaviour indicates the presence of macropores in the adsorbents and these isotherms can be classified as type II [85]. AC_{MW} presents a larger quantity of N_2 adsorbed in comparison with AC/U_{25}, indicating that its structure presents more availability of pores and larger pore volume.

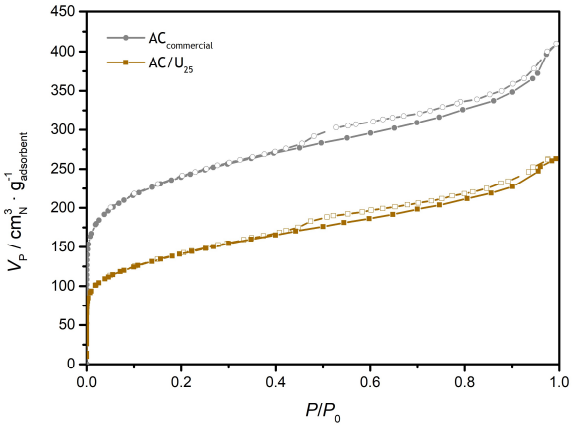

Figure 13. N_2 adsorption-desorption isotherms of $AC_{commercial}$ and AC/U_{25} powders.

Figure 14 shows the N_2 adsorption-desorption isotherms of bares alumina spheres and intact AC-immobilised structures (*i.e.*, without crushing unlike the spectroscopy analyses). It is clear that the amount of N_2 adsorbed increases with the load of urea, but always with a low adsorption of N_2 in the micropore region (*i.e.*, at low relative pressures). These isotherms can be classified as type III. Therefore, after the deposition of the AC materials, there is a markable increase in the N_2 adsorbed, suggesting that the self-immobilised composites are occupying the previously available pores of the bare spheres.

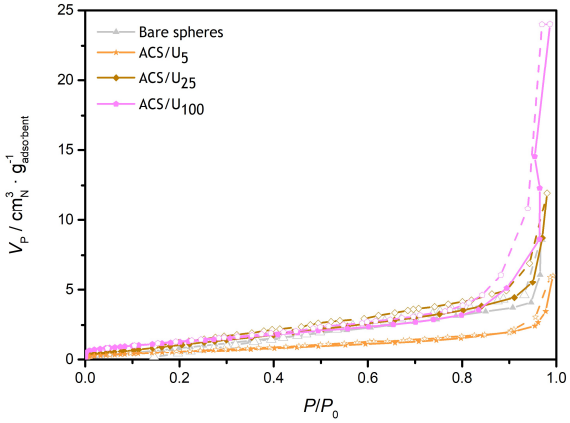

Figure 14. N_2 adsorption-desorption isotherms of bare spheres, ACS/U_5, ACS/U_{25} and ACS/U_{100}.

Regarding the textural properties, **Table 3** shows the S_{BET} and pore volume (V_p) for the selected materials. The S_{BET} of the materials were calculated in the range of relative pressure where monolayer adsorption occurs. $AC_{commercial}$ showed a higher area and pore volume than AC/U_{25}, this can be explained by the occupation of AC/U_{25} pores by urea addition. The S_{BET} calculation for bare spheres, and AC immobilised composites was made considering the range of relative pressures between 0.05-0.20 and the S_{BET} values were always lower than 10 $m^2 \cdot g^-$

[1] $_{adsorbent}$. The pore volume of bare spheres is very low compared with the self-immobilised AC composites; with the pore volume of immobilised composites increasing with the quantity of urea.

Table 3. Specific surface area (S_{BET}) and pore volume (V_p) of $AC_{commercial}$, bare spheres and functionalised AC composites.

Adsorbent	S_{BET} / $m^2 \cdot g_{ads}^{-1}$	V_p / $cm_N^3 \cdot g_{ads}^{-1}$
$AC_{commercial}$	841	0.307
AC/U_{25}	496	0.217
Bare spheres	<10	0.008
ACS/U_5	<10	0.009
ACS/U_{25}	<10	0.018
ACS/U_{100}	<10	0.037

4.1.6. Scanning electron microscopy

The morphological of the selected materials, namely bare spheres, ACS/U_{25}, AC_{MW} and AC/U_{25} were analysed by SEM (**Figure 15**). The respective EDXS spectra are present in **Appendix A.** The bare spheres and ACS/U_{25} were crushed, and the powder structures were used in the analysis as obtained. Bare spheres (**Figure 15a**) show a compacted structure. In the case of ACS/U_{25} (**Figure 15b**), and as attested by DRUV-Vis and PL analysis, some in-grown g-C_3N_4 can be eventually predicted by considering the bright regions. This ACS/U_{25} structure, visually, does not show many similarities with the AC_{MW} structure (**Figure 15c**), but only the ACS/U_{25} material was crushed for this analysis and the resulting particle size is smaller. However, the elemental analysis performed by EDXS in different regions (**Appendix A** and **Table 4**) reveals an increase of carbon content when ACS/U_{25} is compared with the bare spheres, and significantly higher for the other two materials analysed. AC_{MW} and AC/U_{25} (**Figure 15c** and **15d, respectively**) showed several pores and similar, differing in the presence of fluorescent points characteristics of g-C_3N_4 in AC/U_{25} and making its carbon content increase (**Table 4**).

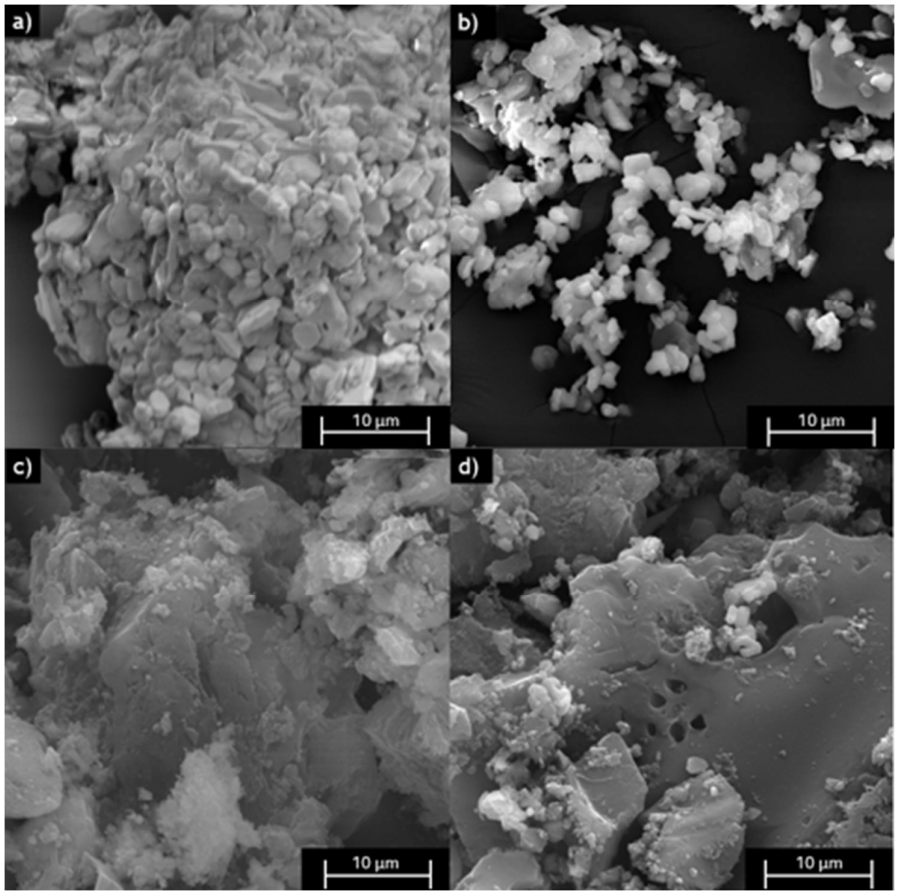

Figure 15. SEM micrographs of: **(a)** bare spheres, **(b)** ACS/U_{25}, **(c)** AC_{MW} *and* **(d)** AC/U_{25}.

Table 4. Elemental composition of the materials obtained by EDXS analysis.

	Spectrum 1			Spectrum 2			Spectrum 3		
	C/%	O/%	Al/%	C/%	O/%	Al/%	C/%	O/%	Al/%
Bare spheres	-----	61.5	38.5	22.4	45.3	32.2	-----	59.4	40.6
ACS/U_{25}	18.9	57.0	24.1	22.8	54.9	22.3	19.0	56.0	25.0
AC_{MW}	88.1	10.4	-----	78.9	17.9	-----	75.8	21.0	-----
AC/U_{25}	95.3	4.7	-----	95.6	4.4	-----	79.3	20.7	-----

4.2. Case Study of Rhodamine B

Trial assays with Rhodamine B (RhB) were carried out to understand the adsorptive capacity of activated carbon, powdered g-C_3N_4, and alumina spheres alone. RhB was chosen as model compound due to its properties as a dye, which is easy to visualise. In this section, the results of the experiments are presented, namely, adsorption evolution, the influence of AC load, the adsorption kinetic and adsorption isotherms.

4.2.1. Rhodamine B adsorption

In RhB adsorption tests with commercial AC, several loads of AC were tested: 0.50, 0.40, 0.35, 0.30, 0.25, 0.10, and 0.05 $g \cdot L^{-1}$ with 50 mL of a 50 ppm RhB aqueous solution. The mixture was firstly sonicated to promote homogenous dispersion of the adsorbent. A full wavelength spectrum was first obtained to select the RhB absorption wavelength for quantification. The highest absorption was measured at 554 nm, and the calibration curve (**Figura A.1**) was obtained accordingly.

As it can be seen in **Figure 16a**, the removal of RhB is rather fast in the first 5 min of contact. For the AC loads between 0.50 and 0.30 $g \cdot L^{-1}$ after 30 minutes of experiment, more than 85% of RhB had been removed. The load of 0.25 $g \cdot L^{-1}$ showed a slower pace of adsorption and allowed to assess RhB evolution for 55 minutes, but also with a removal higher than 50%. Lower loads of AC (0.10 and 0.05 g L^{-1}), shown in **Figure 16b**, represent much lower removal rates of RhB. In comparison, control experiments were performed using bare alumina and powdered g-C_3N_4. The assays with g-C_3N_4 and alumina spheres were made with loads of 2 and 10 $g \cdot L^{-1}$ respectively, these loads were chosen due to the lower adsorption capacities of these materials reported in the literature **Figure 16b** shows a low removal of RhB with both g-C_3N_4 and Al_2O_3 spheres as adsorbents (*ca.* 31% and 18%, respectively).

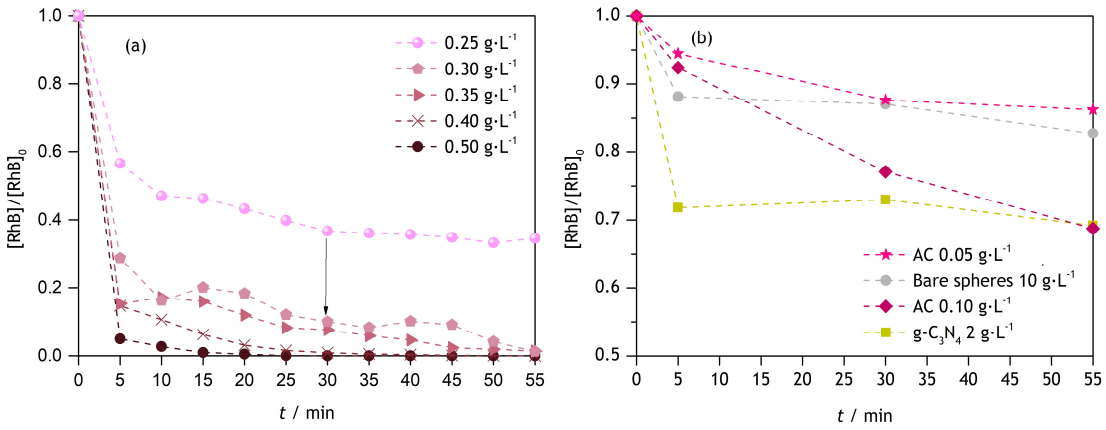

Figure 16. RhB removal at **(a)** loads of powder AC higher or equal than 0.25 $g \cdot L^{-1}$ and **(b)** 0.10 and 0.05 $g \cdot L^{-1}$ of AC, 2 $g \cdot L^{-1}$ of g-C_3N_4, and 10 $g \cdot L^{-1}$ of bare spheres.

4.2.2. Adsorption kinetics of RhB

Since there is no significant removal with g-C_3N_4 or Al_2O_3, the adsorption kinetics were studied only for the AC material, at the intermediate load of 0.25 $g \cdot L^{-1}$. The adsorption kinetic experiments were used to study the rate of adsorbate transfer from the solution to the adsorbent surface and predict the minimum time required. The PFO and PSO were fitted to the data (**Figure 17**). It can be observed that the model which better fit to the

experimental data is PSO (with R^2=0.99 higher than PFO R^2=0.97, **Table 5**), suggesting that chemical adsorption is the rate-limiting step and the absorbent has several active sites [86]. It can be noticed that after 30 minutes, there is almost no additional adsorption, and the equilibrium was reached.

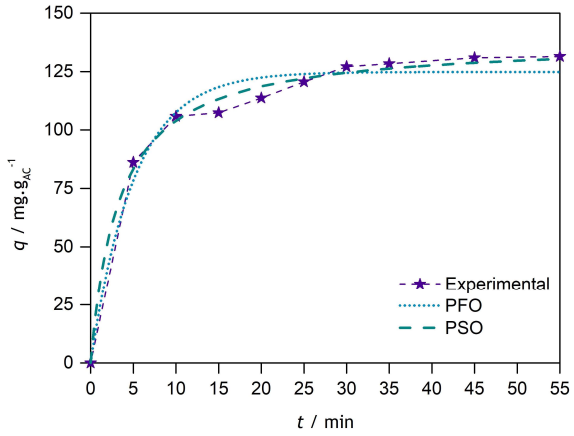

Figure 17. Adsorption kinetics of the experimental using AC_{MW}, with PFO and PSO fitted to experimental data.

Table 5. Adsorption kinetics parameters obtained with PSO and PFO fitting to the experimental data.

Model	q_e/mg·g^{-1}	k_1/min^{-1}	k_2/g·mg^{-1}·min^{-1}	R^2
PFO	124.8	0.198		0.97
PSO	138.2		0.002	0.99

4.2.3. Adsorption isotherms

Adsorption isotherms show the relationship between the adsorbate in aqueous phase and adsorbate accumulation into the adsorbent surface at equilibrium. By fitting the Sips, D-R, Langmuir and Freundlich models to the experimental data (**Figure 18**), Sips showed a higher coefficient of determination (**Table 6**) in comparison with the other models. This suggests that the relation between equilibrium adsorption capacity and equilibrium concentration will be monolayer (Langmuir) at higher adsorbate concentration and multilayer (Freundlich) at lower adsorbate concentrations. Moreover, the D-R isotherm was used to determine if the adsorption process is tendentially physical or chemical, according to the adsorption energy. The value obtained was 1446 kJ·mol^{-1} (parameters used in calculation are in **Table 6**), and according to the literature, if the adsorption energy is higher than 8 kJ·mol^{-1}, the adsorption occurs chemically, if not, physically. Since the obtained value is markedly higher, the adsorption occurs chemically, attesting the assumption obtained from the adsorption

kinetics. However, it is important to claim that none of the models agreed very well to the experimental data.

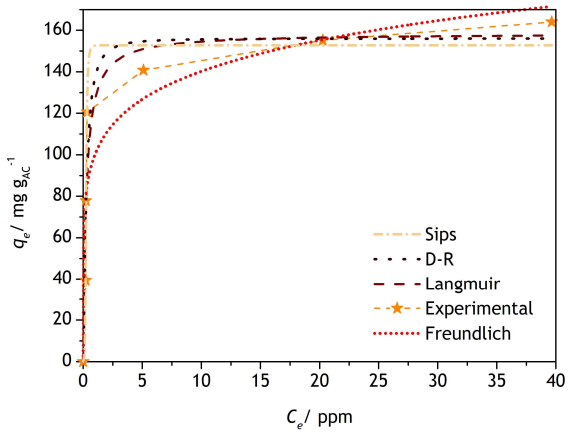

Figure 18. Adsorption isotherms for RhB using AC_{MW}.

Table 6. Adsorption isotherms parameters obtained for RhB.

Model	q_m / mg·g^{-1}	K / L·mg^{-1}	K_F / mg·g^{-1}	K_{DR} / mol^2·kJ^{-2}	Non-dimensional parameter	R^2
Langmuir	158.5	3.9				0.89
Freundlich			100.2		6.9	0.84
Sips	152.8	804.0			4.7	0.96
D-R	156.0			2.4 x 10^{-7}		0.90

4.3. VFX adsorption

4.3.1. AC loads

The selection of the best AC load for this type of study needs to consider the removal evolution of the contaminant as the removal needs to be quantified in a given range, *i.e.* not too fast nor too slow. In **Figure 19**, >99% removal was reached in 10 minutes when using 0.30 and 0.25 g·L^{-1} of AC loads. For 0.10 g·L^{-1}, the removal had a slower adsorption, but in 60 min the equilibrium was achieved. Using 0.05 g·L^{-1}, the equilibrium was not yet reached within 60 min and there was a significant VFX removal (nearly 80%), allowing for proper kinetics evaluation.

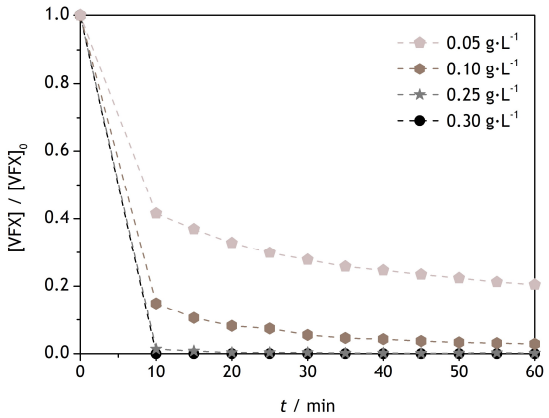

Figure 19. VFX removal by adsorption with different AC loads (0.05 to 0.30 g L^{-1}).

4.3.2. pH influence in VFX removal

The impact of pH in VFX adsorption was studied to better understand the interaction of negative and positive charged VFX within the materials. VFX shows a pK_a of 10.09, indicating that it exists almost entirely in its cationic form at pH values below it. The pH_{PZC} of $AC_{commercial}$ was determined to be around 9.2 (**Figure 12d**), and consequently, lower pH values the AC surface will be positively charged, making difficult the attraction between the VFX cationic species and the AC surface. On the other hand, higher pH values turn the AC surface negatively charged and more attractive for VFX cationic species adsorption via electrostatic interaction (*i.e.*, 9.2 < pH < 10.09). As it can be seen in **Figure 20**, the VFX adsorption increases with the pH value (from 4 to 10). This occurs for the solutions where the pH was obtained from adjustment with HCl and NaOH solutions.

The adsorption in the solution without pH adjustment, with an initial pH of 5.8, the adsorption was quite better than that of the pH 10 solution. This could be explained by the presence of the pH-adjusting salts, that can possibly hinder the adsorption process.

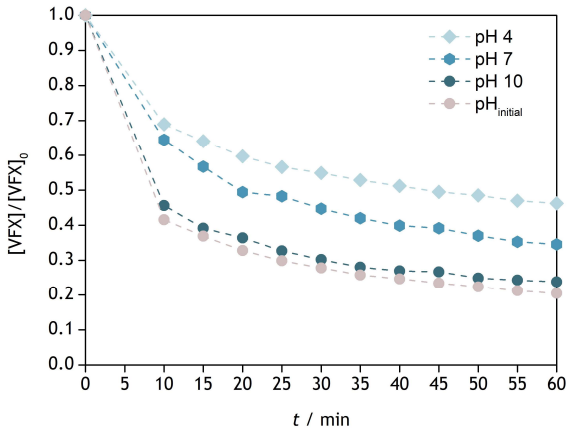

Figure 20. VFX adsorption evolution with time at different pH-adjusted values (4, 7, 10) and unaltered initial pH of 5.8.

4.3.3. AC and functionalised AC composites for VFX adsorption

Thermally-treated AC (AC_{MW}) and the powder functionalised AC composites (AC/U_x) were tested at the same conditions as commercial AC, with a load of 0.10 $g \cdot L^{-1}$. **Figure 21** shows the removal of VFX after 60 min of contact with AC and AC-derived adsorbents. As can be seen, AC_{MW} does not lose activity after the microwave thermal treatment, preserving its adsorption capacity.

The inclusion of *in situ* synthesised g-C_3N_4 onto the AC microstructure makes the adsorption capacity decrease slightly. However, there is no linear relation between AC and urea dosage. Small amounts of urea (AC/U_5) reduce the adsorption capacity compared to bare AC, probably cause of the collapse of active centre micropores. In contrast, when increasing the dosage of urea in the synthesis allows for composites to have greater adsorption until an optimal value (AC/U_{25}), after which there is reduction of the adsorption capacity (**Figure 21**). Hence, it was found that the ideal ratio of AC/U is 50 g_U/g_{AC}, achieved with AC/U_{25} (25 g of urea to 0.5 g of AC).

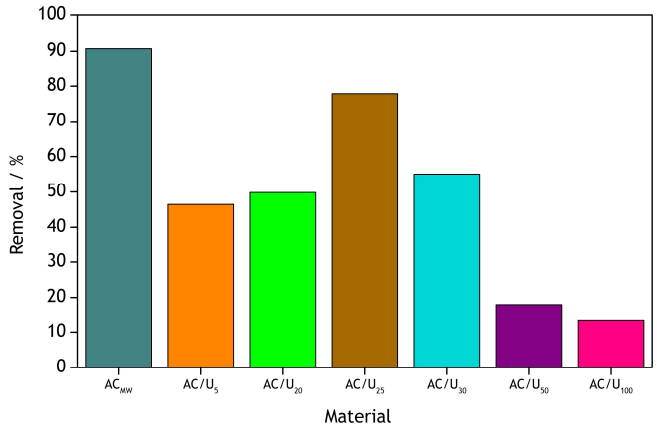

Figure 21. Comparison of VFX removal capacity of AC and its powder composites.

4.3.4. VFX adsorption kinetics of functionalised AC materials

The VFX adsorption kinetic studies were performed in batch mode with two materials: commercial AC at 0.05 $g \cdot L^{-1}$ and AC/U_{25} at 0.10 $g \cdot L^{-1}$. For AC, the kinetic model that better fit the experimental data is PSO, with a R^2 of 0.99 higher than that of PFO with R^2 = 0.97 (**Figure 22**, **Table 7**). This means that the VFX adsorption rate depends on the adsorption capacity and not on concentration of adsorbate, similarly to that obtained with RhB.

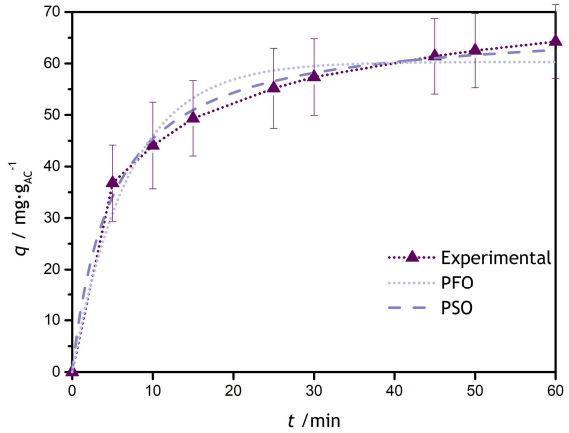

Figure 22. VFX adsorption kinetics with AC as adsorbent (load of 0.05 g L^{-1}).

Table 7. Adsorption kinetics parameters obtained with PSO and PFO fitting to the experimental data with AC as adsorbent.

Model	q_e / mg·g^{-1}	k_1 / min^{-1}	k_2 /g·mg^{-1}·min^{-1}	R^2
PFO	60.3	0.144		0.97
PSO	67.7		0.003	0.99

Figure 23 shows that the urea-functionalised AC did not alter the adsorption kinetics type for VFX adsorption. The best fit is obtained with the PSO model (R^2 of 0.99, while for the PFO model R^2 is 0.98, **Table 8**). The maximum adsorption capacity within 60 minutes with AC/U_{25} as adsorbent decreases significantly (32.7 mg·g^{-1}) in comparison with bare AC (64.2 mg·g^{-1}).

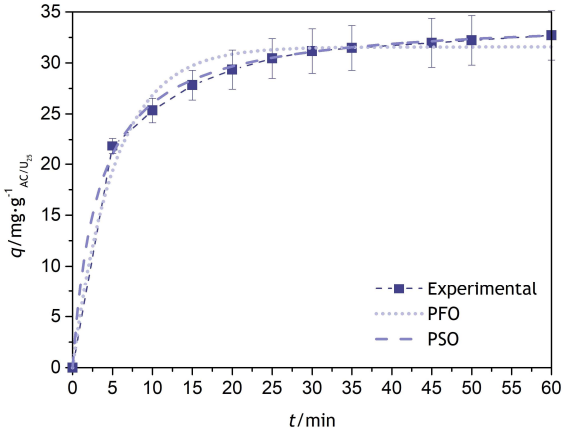

Figure 23. VFX adsorption kinetic with AC/U_{25} as adsorbent.

Table 8. Adsorption kinetics parameters obtained with PSO and PFO fitting to the experimental data with AC/U_{25} as adsorbent.

Model	q_e / mg·g^{-1}	k_1 / min^{-1}	k_2 /g·mg^{-1}·min^{-1}	R^2
PFO	31.2	0.198		0.98
PSO	34.1		0.009	0.99

4.3.5. Adsorption equilibrium

For bare AC, the maximum adsorption capacity was determined to be 69.3 mg·g^{-1}, with the Sips model showing as the best fitting with a R^2 of 0.99 (**Figure 24**, **Table 9**), as in the case of RhB. The adsorption energy value obtained from D-R isotherm was 2707 kJ·mol^{-1}, with a D-R constant of 6.8 × 10^{-8} mol^2 kJ^{-2}, suggesting that the adsorption occurs chemically.

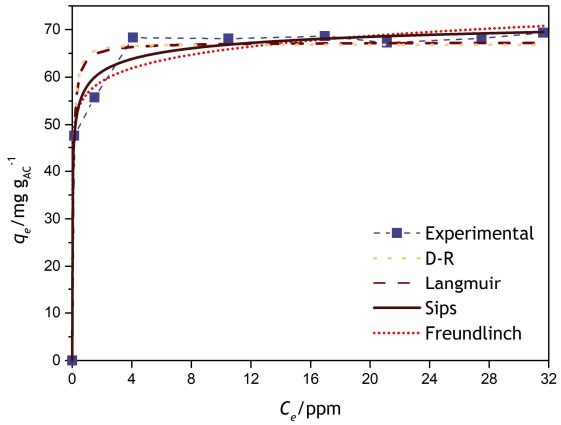

Figure 24. Adsorption isotherms of VFX with bare AC as adsorbent.

Table 9. Adsorption isotherms parameters obtained for VFX with AC as adsorbent.

Model	q_m / mg·g^{-1}	K / L·mg^{-1}	K_F / mg·g^{-1}	K_{DR} / mol^2·kJ^{-2}	Non-dimensional parameter	R^2
Langmuir	67.3	16.8				0.97
Freundlich			56.6		15.4	0.98
Sips	76.1	3.2			0.3	0.99
D-R	66.8			6.8 x 10^{-8}		0.97

Similar to AC, the Sips model with a R^2 = 0.999 fits best to the adsorption equilibrium of VFX with AC/U_{25} as adsorbent (**Figure 25**, **Table 10**). A maximum adsorption capacity of 52.6 mg·g^{-1} was calculated, and an adsorption energy from D-R equation of 468 kJ·mol^{-1} was found, much lower than that obtained with bare AC.

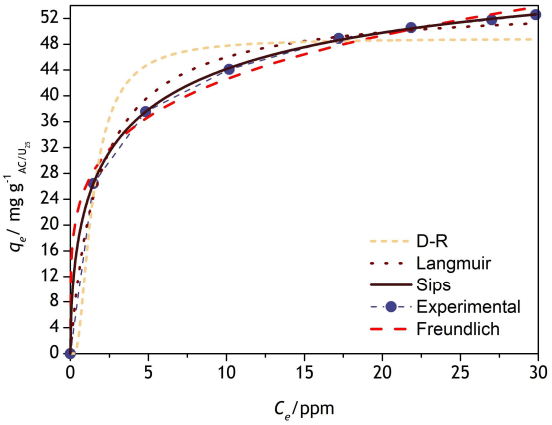

Figure 25. Adsorption isotherms of VFX with AC/U_{25} as adsorbent.

Table 10. Adsorption isotherms parameters obtained for VFX with AC/U_{25} as adsorbent.

Model	q_m / mg·g^{-1}	K / L·mg^{-1}	K_F / mg·g^{-1}	K_{DR} / mol^2·kJ^{-2}	Non-dimensional parameter	R^2
Langmuir	54.3	0.551				0.992
Freundlich			26.1		4.7	0.994
Sips	68.2	0.510			0.6	0.999
D-R	48.9			2.3 x 10^{-6}		0.951

4.3.6. H_2O_2 consumption by AC/U_x

The H_2O_2 measurement allows the validation of CWPO for adsorbent regeneration. Initial assays with H_2O_2 were made to study the catalytic capacity of the functionalised adsorbents. To ensure that neither H_2O_2 is decomposed nor VFX is degraded in presence of that oxidant, a singular assay without any adsorbent addition was performed. The assay attested that the presence of H_2O_2 in VFX solution was negligible for the degradation of VFX (**Figure 26**). The addition of H_2O_2 to experiments with AC (commercial and MW), hinders the adsorption capacity, with the adsorption of VFX being similar or lower in the presence of H_2O_2, likely because of adsorption competition kinetics in the active centres. In contrast, AC/U_{25} shows some catalytic activity, since the removal capacity is slightly improved by the addition of H_2O_2 (**Figure 26**).

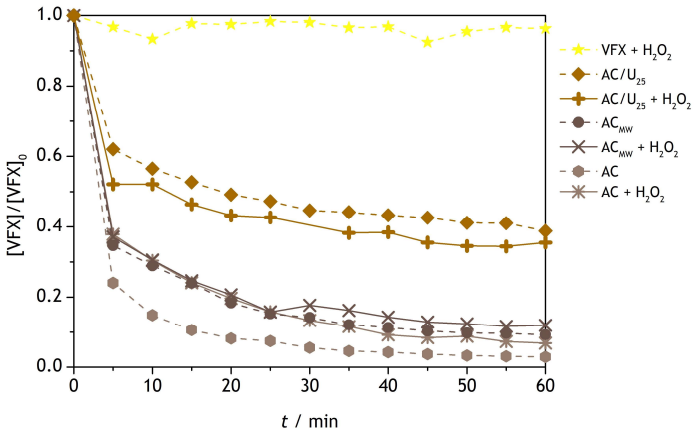

Figure 26. CWPO studies in batch operation mode: adsorption assays with AC_{MW}, $AC_{commercial}$ and AC/U_{25} in the presence and absence of H_2O_2; and control assay with only H_2O_2.

4.3.7. Saturation and regeneration assays

To better understand the adsorption capacity of AC and AC/U_{25}, long-term batch assays were carried out. **Figure 27** shows the evolution of VFX concentration after consequent spikes of VFX every hour, for 5 consecutive cycles, followed by a single long-term 24 h experiment. The first spike was performed after 1 hour of VFX adsorption. After 60 min of adsorption, both adsorbents still showed a satisfactory VFX removal. However, spike by spike the adsorbents become saturated and after 19 h from the last spike, there was no more adsorption on both materials. In addition to the 5-spike experiment with VFX, the same experiment was performed, this time with H_2O_2 addition. Comparing to the other materials, AC reach the equilibrium faster since CWPO did not occur on the bare material. On the other hand, AC/U_{25} showed a more stable behaviour and a higher VFX degradation after 24 h of use, compared to bare AC, owing to the possible catalytic activity of the functionalised material (**Figure 27**).

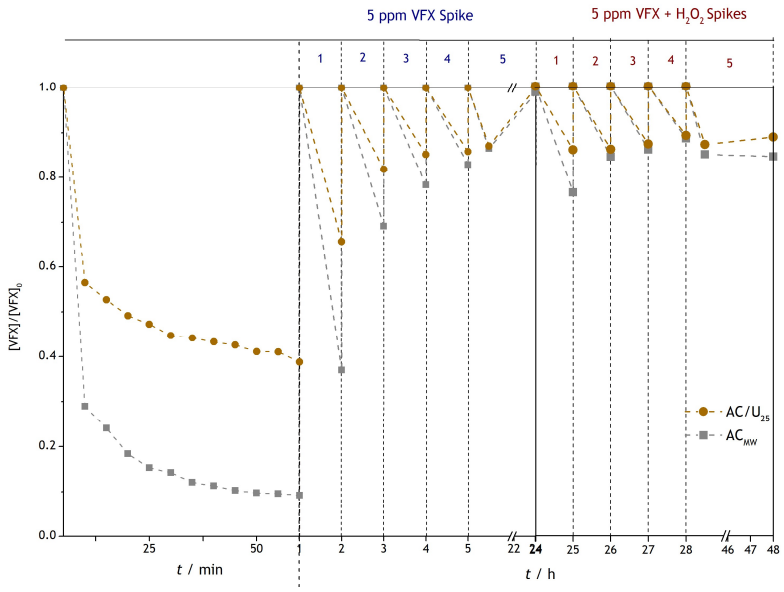

Figure 27. Normalised VFX concentration evolution (1st hour, $[VFX]_0$ = 5 ppm) and after 5 consecutive spikes of 5 ppm of VFX until complete adsorbent saturation and further 5 consecutive spikes of both 5 ppm of VFX and 25 mM H_2O_2.

4.3.8. Continuous mode operation with self-immobilised functionalised AC

Following the previous studies, it is observed that bare AC shows better adsorption capacity than its functionalised composites, using the same adsorbent load (**Figure 21**). However, AC itself does not have the ability to be self-immobilised onto the alumina spheres.

So, to avoid the disadvantages of separating the spent adsorbent from the treated water, assays with alumina spheres coated with AC/U_{20}, AC/U_{25} and AC/U_{30} were carried out in continuous flow mode (**Figure 28**). For comparison purposes, an assay with bare spheres was also performed.

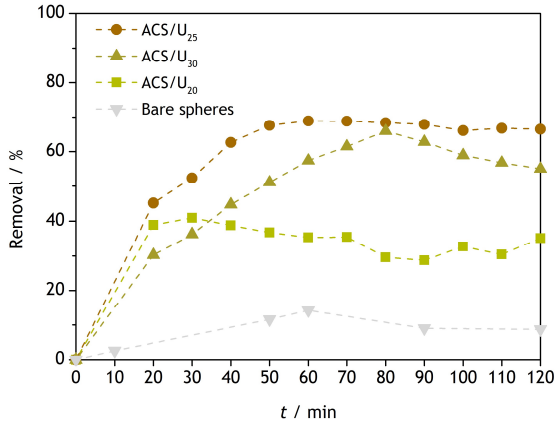

Figure 28. VFX removal under continuous flow mode operation with different ACS/U_x composites and bare spheres, at a flow rate of 0.22 $cm^3 \cdot min^{-1}$.

Firstly, no significant adsorption of VFX was observed with bare spheres, whereas immobilised composite materials show an enhancement in VFX adsorption (ACS/U_{25} =66% > ACS/U_{30} =55 % > ACS/U_{20} = 35%). Therefore, similar to the batch experiments (**Figure 21**), AC/U_{25} proved to outperform the other materials for VFX adsorption. It is suggested that the ACS/U_{20} may have its surface quickly saturated, slowly increasing the VFX concentration at the outlet. Then, ACS/U_{30} reaches its maximum capacity at 80 min of contact but still lower than AC/U_{25}. The best-performing adsorbent ACS/U_{25} shows a nearly exponential decrease until 60 min, after which reaching ~70% removal plateau stable for at least another 60 min. Bare sphere showed non-significant VFX removal. It is expectable that after a few hours the outlet concentration starts to increase due to saturation of the adsorbent, for calidation, longer duration experiments are necessary.

4.3.9. H_2O_2 consumption by ACS/U_x

To understand the ability of these materials to activate H_2O_2, aqueous solutions of H_2O_2 were pumped into the reactor loaded with ACS/U_x materials. The concentration of H_2O_2 was followed during the experiment to assess the consumption/activation of the oxidation by the functionalised AC materials and validate the CWPO process for possible regeneration experiments. These tests were performed with the supported spheres with higher adsorption performance (*i.e.*, ACS/U_{20}, ACS/U_{25} and ACS/U_{30}) and bare spheres for comparison purposes (**Table 11**, **Figure 29**). Bare spheres showed a slight H_2O_2 consumption, although, the H_2O_2 was not applied in CWPO for VFX degradation, since the removal is lower than the removal in the experiment without H_2O_2. Most probably, the bare spheres decompose H_2O_2 without radicals' formation. The increase of VFX in the outlet solution could also be explained by a possible competition between H_2O_2 and VFX. Possibly, when H_2O_2 is added to the inlet solution it occupies centres previously occupied by VFX in the spheres since it was seen the bare alumina has a high affinity towards H_2O_2 decomposition.

The consumption of H_2O_2 by immobilised AC composites seems to be related to the adsorbate quantity (more adsorbate, more H_2O_2 is needed), while the VFX degradation with H_2O_2 increased with the urea content in functionalised AC materials (**Figure 29**). So, immobilised materials could be regenerated via CWPO.

Table 11. Values of H_2O_2 absorbance before and after CWPO and VFX removal in presence of H_2O_2 after 1 hour and maximum removal in absence of H_2O_2.

	H_2O_2 Consumption (%)	Removal of VFX (%) in the presence of H_2O_2	Removal of VFX (%) without H_2O_2
Bare spheres	71.1	10	15
ACS/U_{20}	91.8	62	41
ACS/U_{25}	94.4	75	69
ACS/U_{30}	85.0	81	66

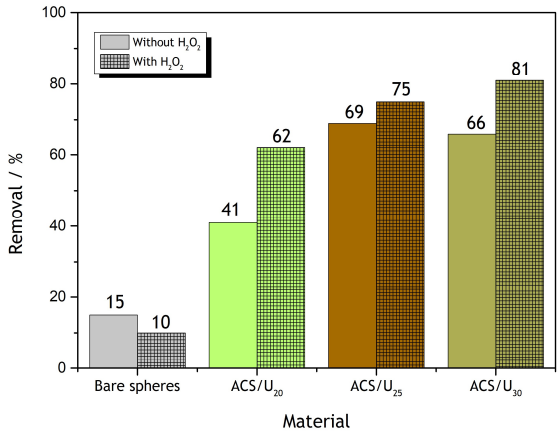

Figure 29. Comparison between the removal of VFX by 3D materials in the presence and absence of H_2O_2.

4.3.10. Adsorption of VFX spiked in tap water

In order to operate with more realistic conditions, VFX was spiked onto potable tap water. The assays were carried out under the same continuous mode conditions. **Figure 30** shows the comparison between the UP and drinking water matrices. As can be seen, VFX adsorption onto ACS/U_{25} surface was higher when drinking water was used as matrix. The VFX solution in UP water showed a pH of 5.8 and the drinking water has a pH near 7.6. Considering ACS/U_{25} pH_{PZC} (7.6), at pH value of 5.8 the adsorbent is positively charged, corresponding to repulsive forces between the adsorbent surface and the VFX cationic species. Increasing the solution pH makes the adsorbent surface become less positively charged, as in the case of drinking water as matrix. The trend also can be explained by the composition of drinking water which include specific inorganic salts that may facilitate the contact between the surface of ACS/U_{25} and VFX. In both cases, the adsorbent reaches the maximum VFX removal after 80 minutes, removing around 78% of VFX in drinking water.

Exploring the advantage of CWPO, as plausible technology to avoid the saturation of the materials the experiments were made with 25 mM H_2O_2 concentration in inlet solution. In both cases is possible to see that the addition of H_2O_2 degrades some VFX. In UP matrix, the CWPO-assisted removal is maintained around 22%, meaning the functionalised ACS/U material activates H_2O_2 and prevents adsorbent saturation. Before the spikes of H_2O_2, there was an upward trend in the VFX concentration which does not occur after CWPO. In the drinking water matrix, owing to interactions with trace inorganic matter, the removal of VFX after 1 h was very high, possibly due to interactions between inorganic salts and H_2O_2 activation. After 2 and 4 h, the VFX removal was maintained at around 50%, meaning the H_2O_2-rich inlet is also preventing adsorbent saturation through continuous CWPO.

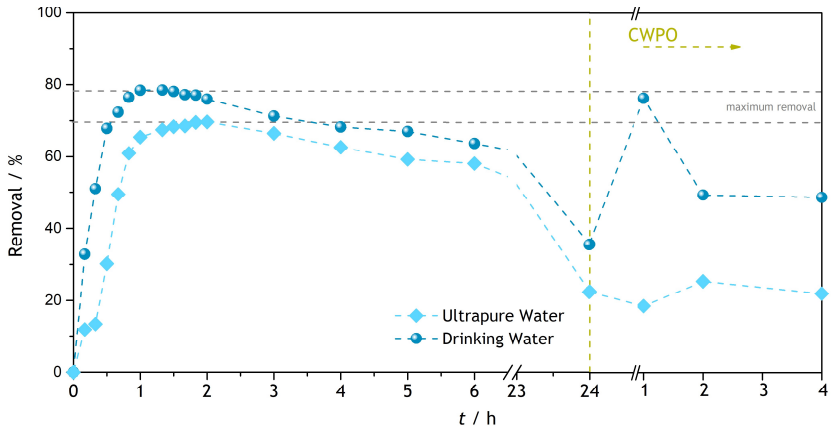

Figure 30. Drinking and UP water matrices spiked with VFX (5 ppm) in adsorption (first 24 h) and CWPO (after 24 h) in continuous flow mode, at a flow rate of 0.22 $cm^3 \cdot min^{-1}$, with ACS/U_{25} at room temperature.

5. Conclusion

The synthesis of functionalised AC with urea, a precursor of g-C_3N_4, was successful for the self-immobilisation of those materials onto three-dimensional alumina structures. This created an adsorbent macrostructure to operate under continuous flow mode. The batch and continuous flow experiments for VFX removal demonstrated that the relation between AC/U and adsorption performance reaches an optimal value of AC/U ratio. Moreover, considering spectroscopy and N_2 adsorption characterisation results, the interaction between urea, AC and alumina spheres was confirmed and the combination of these materials can be seen for different urea dosages.

The functionalised AC composite with best adsorption performance was that with 25 g of urea per 0.500 mg of AC. The powdered composite was tested in batch mode for VFX adsorption: the kinetic data were better fitted by PSO kinetic with R^2=0.99 and the isotherm which better fit to the experimental data was the Sips isotherm with a R^2=999.

The self-immobilised composite of ACS/U_{25} was tested in continuous flow mode in two different matrices: UP water and drinking water from tap. This experiment attested that the composite saturate after 80 minutes with a VFX removal of 78% in drinking water. It was showed that higher pH values improve the adsorption performance of the composite as well the inorganic salts presence, according to the measurements of point of zero charge.

The functionalised AC composite also showed catalytic performance, in contrast to the bare AC material. Therefore, the functionalisation technique allows the recovery of spent adsorbents by adding hydrogen peroxide (CWPO process at room temperature).

6. Assessment of the work done

6.1. Objectives Achieved

The main objective was to synthesise functionalised AC composites and perform the self-immobilisation onto 3D alumina structures for VFX removal from water. To accomplish this goal, several short-term objectives were proposed to: 1) assess the adsorption capacity of the modified AC materials by selecting the best proportion of AC and urea (precursor for g-C_3N_4); 2) immobilise the AC-based composites onto macrostructured alumina spheres; 3) investigate the influence of the water matrix on the adsorption mechanism; and 4) employ catalytic wet peroxide oxidation (CWPO) for the regeneration of spent adsorbents.

1) The best proportion of AC and urea selected was 50 g_{urea}/g_{AC};
2) All the AC-based composites were immobilised onto macrostructured alumina spheres;
3) A water matrix with high pH values and presence of inorganic salts can improve the adsorption capacity of AC-based composites;
4) CWPO was performed but will needs further improvements such as the optimization of hydrogen peroxide concentration and the addition of light to the system.

6.2. Contribution to the Sustainable Development Goals

SDG	Goal	Contribution	Performance and metric indicator
6	1	Development of water purification techniques for micropollutants removal.	Proportion of population using safely managed drinking water services.

6.3. Other Work Carried Out

In sideline with this project, assays with diclofenac and pharmaceuticals in a mixture were made with AC as adsorbent, to assess the efficacy of this adsorption system. The pH study with these matrices was also made.

AC-based composite materials were synthesised in another muffle with conventional heating to verify the synthesis conditions impact, while assays with these materials were also carried out. The materials characterisation, namely, TGA and XRD were made for some AC-based composite materials.

The preparation of abstracts for national and international conferences were prepared for both poster and oral communications.

Oral communication:

- A. Torres-Pinto, **J.J.M. Dele**, A. M. Chávez, A.M.T. Silva, "Self-immobilisation of functional activated carbon on alumina beads for mineral water treatment", 7th

International Congress on Water, Waste and Energy Management (WWEM-24), Lisbon, Portugal, 24-26 July 2024.

Poster communications:

- A. Torres-Pinto, **J.J.M. Dele**, A. M. Chávez, A.M.T. Silva, "Tailoring activated carbon supported on 3D alumina macrospheres for micropollutant adsorption", 43rd Iberian Adsorption Meeting (RIA43), Porto, Portugal, 1-4 September 2024
- A. Torres-Pinto, **J.J.M. Dele**, A. M. Chávez, A.M.T. Silva, "Novel functionalised carbon-based macrostructures for water purification", Winter School on Contaminants of Emerging Concern (CECs) and Disinfection By-Products (DBPs): Occurrence, Impact and Elimination, Vila Nova de Gaia, Portugal, 25-26 November 2024.

6.4. Final Assessment

The development of this work was rather interesting, as it was great and exciting to see the birth of novel adsorbents, test each one and see all the results. However, this work could be improved, since more time would allow:

- a deeper study about the adsorbent's regeneration;
- develop a novel AC from scratch and use it in the synthesis of AC functionalised composites;
- explore other structures for immobilisation;
- perform other adsorbent characterisation techniques;
- make assays with other water matrices, such as river water and seawater;
- better explore the influence of pH in the adsorption process;
- analyse the total organic carbon content before and after the adsorption process;
- explore the composites in other AOPs processes as catalysts.

7. References

[1] W. Musie, G. Gonfa, Fresh water resource, scarcity, water salinity challenges and possible remedies: A review, Heliyon, 9 (2023) 18685.

[2] M. Denchak, Water pollution: everything you need to know, Nat. Resour. Def. Counc. NY, 2023.

[3] J.A. Khan, S. Jabin, 21 - Nanocomposites for the removal of pharmaceuticals in drinking water sources, in: M.E. Khan, J. Aslam, C. Verma (Eds.) Nanocomposites-Advanced Materials for Energy and Environmental Aspects, Woodhead Publishing 2023, pp. 469.

[4] J.P. Bavumiragira, J.n. Ge, H. Yin, Fate and transport of pharmaceuticals in water systems: A processes review, Science of The Total Environment, 823 (2022) 153635.

[5] D. Simazaki, R. Kubota, T. Suzuki, M. Akiba, T. Nishimura, S. Kunikane, Occurrence of selected pharmaceuticals at drinking water purification plants in Japan and implications for human health, Water Research, 76 (2015) 187.

[6] J. Bednárek, P. Šiler, J. Švec, M. Vráblová, Use of thermal analysis for the study of the adsorption of pharmaceuticals from water, Surfaces and Interfaces, 46 (2024) 104065.

[7] H. Yu, Y. Zhang, C. Xing, Y. Wang, H. Zhang, N. Gong, Y. Lu, G. Du, Venlafaxine caffeic acid salt: Synthesis, structural characterization, and hypoglycemic effect analysis, ACS omega, 6 (2021) 13895.

[8] M. Llorca, F. Castellet-Rovira, M.-J. Farré, A. Jaén-Gil, M. Martínez-Alonso, S. Rodríguez-Mozaz, M. Sarrà, D. Barceló, Fungal biodegradation of the N-nitrosodimethylamine precursors venlafaxine and O-desmethylvenlafaxine in water, Environmental Pollution, 246 (2019) 346.

[9] L.P.d. Souza, F.O. Sanches-Neto, G.M.Y. Junior, B. Ramos, A.M. Lastre-Acosta, V.H. Carvalho-Silva, A.C.S.C. Teixeira, Photochemical environmental persistence of venlafaxine in an urban water reservoir: A combined experimental and computational investigation, Process Safety and Environmental Protection, 166 (2022) 478.

[10] A.L.S. Vieira, R.S. Ribeiro, A.R. Lado Ribeiro, A.M. Ribeiro, A.M.T. Silva, Hollow carbon spheres for diclofenac and venlafaxine adsorption, Journal of Environmental Chemical Engineering, 10 (2022) 107348.

[11] J. Xu, Y. Yuan, W. Zhang, C. Liu, Z. Wang, J. Li, The adsorption and its mechanism of venlafaxine by original and aged polypropylene microplastic and the changes of joint toxicity, Journal of Environmental Management, 353 (2024) 120176.

[12] M.J. García-Galán, A. Anfruns, R. Gonzalez-Olmos, S. Rodríguez-Mozaz, J. Comas, UV/H_2O_2 degradation of the antidepressants venlafaxine and O-desmethylvenlafaxine: elucidation of their transformation pathway and environmental fate, Journal of Hazardous Materials, 311 (2016) 70.

[13] M. Voigt, J.M. Dluziak, N. Wellen, V. Langerbein, M. Jaeger, Comparison of photoinduced and electrochemically induced degradation of venlafaxine, Environmental Science and Pollution Research, 31 (2024) 13442.

[14] J.C. Aldana, M. Pedrosa, A.M.T. Silva, J.L. Faria, J.L. Acero, P.M. Álvarez, Nanocomposite PVDF/TiO_2 Photocatalytic Membranes for Micropollutant Removal in Secondary Effluent, Catalysts, 14 (2024) 109.

[15] K. Kaya-Özkiper, A. Uzun, S. Soyer-Uzun, Boosting methylene blue adsorption capacity of an industrial waste-based geopolymer by depositing graphitic carbon nitride onto its surface: Towards sustainable materials for wastewater treatment, Chemical Engineering Science, 284 (2024) 119398.

[16] M. Alaqarbeh, Adsorption phenomena: definition, mechanisms, and adsorption types: short review, RHAZES: Green and Applied Chemistry, 13 (2021) 43.

[17] K. Kaya-Özkiper, A. Uzun, S. Soyer-Uzun, A novel alkali activated magnesium silicate as an effective and mechanically strong adsorbent for methylene blue removal, Journal of Hazardous Materials, 424 (2022) 127256.

[18] K. Kaya-Özkiper, A. Uzun, S. Soyer-Uzun, Red mud-and metakaolin-based geopolymers for adsorption and photocatalytic degradation of methylene blue: Towards self-cleaning construction materials, Journal of Cleaner Production, 288 (2021) 125120.

[19] H. Khan, S. Hussain, R. Zahoor, M. Arshad, M. Umar, M.A. Marwat, A. Khan, J.R. Khan, M.A. Haleem, Novel modeling and optimization framework for Navy Blue adsorption onto eco-friendly magnetic geopolymer composite, Environmental Research, 216 (2023) 114346.

[20] F. Largo, R. Haounati, S. Akhouairi, H. Ouachtak, R. El Haouti, A. El Guerdaoui, N. Hafid, D.M. Santos, F. Akbal, A. Kuleyin, Adsorptive removal of both cationic and anionic dyes by using sepiolite clay mineral as adsorbent: Experimental and molecular dynamic simulation studies, Journal of Molecular Liquids, 318 (2020) 114247.

[21] W.S. Chai, J.Y. Cheun, P.S. Kumar, M. Mubashir, Z. Majeed, F. Banat, S.-H. Ho, P.L. Show, A review on conventional and novel materials towards heavy metal adsorption in wastewater treatment application, Journal of Cleaner Production, 296 (2021) 126589.

[22] T. Gao, S. Yu, H. Wang, X. Zhao, C. Wang, S. Xiao, MOFs-based photocatalytic self-cleaning membranes for highly efficient wastewater treatment: A review, Chemical Engineering Science, 278 (2023) 118891.

[23] R. Shu, Q. Qiao, F. Guo, K. Dong, S. Liu, L. Xu, Y. Bai, N. Zhou, Controlled design of Na-P1 zeolite/porous carbon composites from coal gasification fine slag for high-performance adsorbent, Environmental Research, 217 (2023) 114912.

[24] J. Karuppaiyan, A. Mullaimalar, R. Jeyalakshmi, Adsorption of dyestuff by nano copper oxide coated alkali metakaoline geopolymer in monolith and powder forms: Kinetics, isotherms and microstructural analysis, Environmental Research, 218 (2023) 115002.

[25] M. Fronczak, Adsorption performance of graphitic carbon nitride-based materials: Current state of the art, Journal of Environmental Chemical Engineering, 8 (2020) 104411.

[26] F.S. Baker, C.E. Miller, A.J. Repik, E.D. Tolles, Activated carbon, Kirk-Othmer Encyclopedia of Chemical Technology, 4 (1992) 1015.

[27] J.R. de Andrade, M.F. Oliveira, M.G.C. da Silva, M.G.A. Vieira, Adsorption of pharmaceuticals from water and wastewater using nonconventional low-cost materials: a review, Industrial & Engineering Chemistry Research, 57 (2018) 3103.

[28] B. Zhu, P. Xia, W. Ho, J. Yu, Isoelectric point and adsorption activity of porous g-C_3N_4, Applied Surface Science, 344 (2015) 188.

[29] A.M. Chávez, A. Torres-Pinto, P.M. Álvarez, J.L. Faria, C.G. Silva, A.M.T. Silva, One-pot synthesis and immobilization of urea-derived graphitic carbon nitride onto ceramic foams for visible-light photocatalytic wet peroxide oxidation in water treatment, Chemical Engineering Journal, 481 (2024) 148141.

[30] M. Andrés Gallardo Salas, D. Ileana Mendoza-Castillo, A. Bonilla-Petriciolet, C. Jiménez-Junca, Functionalized activated carbon with whey protein amyloid fibrils for adsorption of arsenic from water, Environmental Nanotechnology, Monitoring and Management, 22 (2024) 100956.

[31] A. Bhatnagar, W. Hogland, M. Marques, M. Sillanpää, An overview of the modification methods of activated carbon for its water treatment applications, Chemical Engineering Journal, 219 (2013) 499.

[32] F. Rodríguez-Reinoso, Activated Carbon and Adsorption, in: K.H.J. Buschow, R.W. Cahn, M.C. Flemings, B. Ilschner, E.J. Kramer, S. Mahajan, P. Veyssière (Eds.) Encyclopedia of Materials: Science and Technology, Elsevier, Oxford, 2001, pp. 22.

[33] P. Chingombe, B. Saha, R.J. Wakeman, Surface modification and characterisation of a coal-based activated carbon, Carbon, 43 (2005) 3132.

[34] Y. Jari, N. Roche, M. Chaker Necibi, F. Zahra Falil, S. Tayibi, K. Lyamlouli, A. Chehbouni, B. Gourich, Porous activated carbons derived from waste Moroccan pine cones for high-performance adsorption of bisphenol A from water, Heliyon, 10 (2024) 29645.

[35] A. Drenkova-Tuhtan, C.S. Inskeep, L. Luthardt, S.L. Deuso, T. Ballweg, D. Hanselmann, Z. Béalu, C. Meyer, B. Schug, H. Steinmetz, K. Mandel, Reusable and inductively regenerable magnetic activated carbon for removal of organic micropollutants from secondary wastewater effluents, Water Research, 255 (2024) 121525.

[36] P. Pietrowski, I. Ludwiczak, J. Tyczkowski, Activated carbons modified by Ar and CO_2 plasmas - Acetone and cyclohexane adsorption, Medziagotyra, 18 (2012) 158.

[37] M. Wei, L. Gao, J. Li, J. Fang, W. Cai, X. Li, A. Xu, Activation of peroxymonosulfate by graphitic carbon nitride loaded on activated carbon for organic pollutants degradation, Journal of Hazardous Materials, 316 (2016) 60.

[38] A. Torres-Pinto, C.G. Silva, J.L. Faria, A.M.T. Silva, The effect of precursor selection on the microwave-assisted synthesis of graphitic carbon nitride, Catalysis Today, 424 (2023) 113868.

[39] M.J. Lima, A.M.T. Silva, C.G. Silva, J.L. Faria, Graphitic carbon nitride modified by thermal, chemical and mechanical processes as metal-free photocatalyst for the selective synthesis of benzaldehyde from benzyl alcohol, Journal of Catalysis, 353 (2017) 44.

[40] A. Ahmadi, M. Hajilou, S. Zavari, S. Yaghmaei, A comparative review on adsorption and photocatalytic degradation of classified dyes with metal/non-metal-based modification of graphitic carbon nitride nanocomposites: Synthesis, mechanism, and affecting parameters, Journal of Cleaner Production, 382 (2023) 134967.

[41] L. Zhang, L. Li, X. Sun, P. Liu, D. Yang, X. Zhao, ZnO-Layered double Hydroxide@Graphitic Carbon nitride composite for consecutive Adsorption and photodegradation of dyes under UV and visible lights, Materials, 9 (2016) 927.

[42] S. Haydar, M.A. Ferro-García, J. Rivera-Utrilla, J.P. Joly, Adsorption of p-nitrophenol on an activated carbon with different oxidations, Carbon, 41 (2003) 387.

[43] B. Ren, Y. Xu, L. Zhang, Z. Liu, Carbon-doped graphitic carbon nitride as environment-benign adsorbent for methylene blue adsorption: Kinetics, isotherm and thermodynamics study, Journal of the Taiwan Institute of Chemical Engineers, 88 (2018) 114.

[44] A.R.S. Nazar, M.B. Kurade, M.A. Khan, B.H. Jeon, Effect of humic acid on adsorption of methylparaben from aqueous solutions onto commercially available granular activated carbons, Scientia Iranica, 29 (2022) 1364.

[45] K.C. Lai, L.Y. Lee, B.Y.Z. Hiew, S. Thangalazhy-Gopakumar, S. Gan, Environmental application of three-dimensional graphene materials as adsorbents for dyes and heavy metals: Review on ice-templating method and adsorption mechanisms, Journal of Environmental Sciences, 79 (2019) 174.

[46] L. Zhao, W. Lv, J. Hou, Y. Li, J. Duan, S. Ai, Synthesis of magnetically recyclable g-C_3N_4/Fe_3O_4/ZIF-8 nanocomposites for excellent adsorption of malachite green, Microchemical Journal, 152 (2020) 104425.

[47] Y. Wang, L. He, G. Dang, H. Li, X. Li, Preparation of Fe-MIL(100)-encapsulated magnetic g-C_3N_4 for adsorption of PPCPs from aqueous solution, Environmental Science and Pollution Research, 28 (2021) 39769.

[48] A. Abushawish, I.W. Almanassra, A.D. Manasrah, A. Shanableh, M. Ali Atieh, In-depth analysis of MgAl layered double oxide AC composite for sulfate removal from United Arab Emirates Ground Water: Synthesis optimization, fixed-bed performance, and economic feasibility, Separation and Purification Technology, 347 (2024) 127594.

[49] X. Wan, M.A. Khan, F. Wang, M. Xia, W. Lei, S. Zhu, C. Fu, Y. Ding, Facile synthesis of protonated g-C_3N_4 and acid-activated montmorillonite composite with efficient adsorption capacity for PO_4^{3-} and Pb(II), Chemical Engineering Research and Design, 152 (2019) 95.

[50] S. Pei, Y. Hu, Y. Huang, Y. Liu, H. Zhou, Ultrasonically assisted synthesis of g-C_3N_4-activated carbon composite for enhanced defluoridation of water, Alexandria Engineering Journal, 86 (2024) 399.

[51] A. Torres-Pinto, A.M. Díez, C.G. Silva, J.L. Faria, M.Á. Sanromán, A.M.T. Silva, M. Pazos, Photoelectrocatalytic degradation of pharmaceuticals promoted by a metal-free g-C_3N_4 catalyst, Chemical Engineering Journal, 476 (2023) 146761.

[52] Z. Cheng, L. Ling, J. Fang, C. Shang, Visible light-driven g-C_3N_4 peroxymonosulfate activation process for carbamazepine degradation: Activation mechanism and matrix effects, Chemosphere, 286 (2022) 131906.

[53] B. Liu, M. Qiao, Y. Wang, L. Wang, Y. Gong, T. Guo, X. Zhao, Persulfate enhanced photocatalytic degradation of bisphenol A by g-C_3N_4 nanosheets under visible light irradiation, Chemosphere, 189 (2017) 115.

[54] W. Lu, L. Qi, D. Dong, X. Shen, L. Xu, Y. Zhang, X. Mei, W. Qiao, X. Guo, Y. Pan, A comparison study of photocatalytic performance of g-C_3N_4 prepared from different precursors for the activation of different peroxides, Separation and Purification Technology, 327 (2023) 124904.

[55] Y. Cui, Z. Ding, P. Liu, M. Antonietti, X. Fu, X. Wang, Metal-free activation of H_2O_2 by g-C_3N_4 under visible light irradiation for the degradation of organic pollutants, Physical Chemistry Chemical Physics, 14 (2012) 1455.

[56] G. Liao, D. Zhu, L. Li, B. Lan, Enhanced photocatalytic ozonation of organics by g-C_3N_4 under visible light irradiation, Journal of Hazardous Materials, 280 (2014) 531.

[57] A. Torres-Pinto, A.R.T. Fernandes, C.G. Silva, J.L. Faria, A.M.T. Silva, The role of added oxidising agents in assisting the photocatalytic treatment of olive mill wastewater using a metal-free g-C_3N_4 optical semiconductor, Journal of Water Process Engineering, 58 (2024) 104722.

[58] C. Kim, H. Yoo, G. Lee, H.J. Hong, Powdered activated carbon (PAC)-assisted peroxymonosulfate activation for efficient urea elimination in ultrapure water production from reclaimed water, Scientific Reports, 14 (2024) 4597.

[59] P. Tan, N. Meng, X. Cao, X. Zhang, Y. Huang, T. Li, W. Wang, Synthesis of integrated material with activation and oxidation functions by mechanical milling of activated carbon and persulfate for enhanced tetracycline degradation over non-radical mechanism, Processes, 12 (2024) 672.

[60] D.A. Gkika, A.C. Mitropoulos, G.Z. Kyzas, Why reuse spent adsorbents? The latest challenges and limitations, Science of The Total Environment, 822 (2022) 153612.

[61] A.V. Baskar, N. Bolan, S.A. Hoang, P. Sooriyakumar, M. Kumar, L. Singh, T. Jasemizad, L.P. Padhye, G. Singh, A. Vinu, B. Sarkar, M.B. Kirkham, J. Rinklebe, S. Wang, H. Wang, R. Balasubramanian, K.H.M. Siddique, Recovery, regeneration and sustainable management of spent adsorbents from wastewater treatment streams: A review, Science of The Total Environment, 822 (2022) 153555.

[62] E. Da'na, A. Awad, Regeneration of spent activated carbon obtained from home filtration system and applying it for heavy metals adsorption, Journal of Environmental Chemical Engineering, 5 (2017) 3091.

[63] X.N. Zhang, G.Y. Mao, Y.B. Jiao, Y. Shang, R.P. Han, Adsorption of anionic dye on magnesium hydroxide-coated pyrolytic bio-char and reuse by microwave irradiation, International Journal of Environmental Science and Technology, 11 (2014) 1439.

[64] S. Tamjidi, H. Esmaeili, B. Kamyab Moghadas, Application of magnetic adsorbents for removal of heavy metals from wastewater: A review study, Materials Research Express, 6 (2019) 102004.

[65] S.Y. Hwang, G.B. Lee, J.H. Kim, B.U. Hong, J.E. Park, Pre-treatment methods for regeneration of spent activated carbon, Molecules, 25 (2020) 4561.

[66] M. Shahadat, S. Isamil, Regeneration performance of clay-based adsorbents for the removal of industrial dyes: a review, RSC advances, 8 (2018) 24571.

[67] D. Jiang, B. Chu, Y. Amano, M. Machida, Removal and recovery of phosphate from water by Mg-laden biochar: Batch and column studies, Colloids and Surfaces A: Physicochemical and Engineering Aspects, 558 (2018) 429.

[68] V. Acevedo-García, E. Rosales, A. Puga, M. Pazos, M.A. Sanromán, Synthesis and use of efficient adsorbents under the principles of circular economy: Waste valorisation and electroadvanced oxidation process regeneration, Separation and Purification Technology, 242 (2020) 116796.

[69] S.M. Mohammed, S. Shukla, Regeneration and recycling of hydrogen titanate nanotubes as methylene blue adsorbent via ozonation-based advanced oxidation process, Water, Air, and Soil Pollution, 234 (2023) 663.

[70] V. Abromaitis, V. Racys, P. van der Marel, R.J.W. Meulepas, Biodegradation of persistent organics can overcome adsorption-desorption hysteresis in biological activated carbon systems, Chemosphere, 149 (2016) 183.

[71] P. Kumari, A. Kumar, ADVANCED OXIDATION PROCESS: A remediation technique for organic and non-biodegradable pollutant, Results in Surfaces and Interfaces, 11 (2023) 100122.

[72] J.J. Rueda Márquez, I. Levchuk, M. Sillanpää, Application of catalytic wet peroxide oxidation for industrial and urban wastewater treatment: a review, Catalysts, 8 (2018) 673.

[73] T. Zhu, J. Deng, S. Zhu, A. Cai, C. Ye, X. Ling, H. Guo, Q. Wang, X. Li, Kinetic and mechanism insights into the degradation of venlafaxine by UV/chlorine process: a modelling study, Chemical Engineering Journal, 431 (2022) 133473.

[74] E.M. El-Fawal, S.A. Younis, T. Zaki, Designing $AgFeO_2$-graphene/$Cu_2(BTC)_3$ MOF heterojunction photocatalysts for enhanced treatment of pharmaceutical wastewater under sunlight, Journal of Photochemistry and Photobiology A: Chemistry, 401 (2020) 112746.

[75] J. Nieto-Sandoval, A. Torres-Pinto, M. Pedrosa, M. Munoz, Z.M. de Pedro, C.G. Silva, J.L. Faria, J.A. Casas, A.M.T. Silva, Application of g-C_3N_4-PVDF membrane for the photocatalytic degradation of micropollutants in continuous flow mode: Impact of water matrix, Journal of Environmental Chemical Engineering, 11 (2023) 110586.

[76] M. Medykowska, M. Wiśniewska, K. Szewczuk-Karpisz, M. Galaburda, Adsorption capacity of carbon-silica composites towards diclofenac in poly(acrylic acid) containing systems: a crucial study on common wastewater contaminants, ChemPhysChem, 25 (2024) 202300813.

[77] D.S. Moura, C.J. Pestana, C.F. Moffat, N. Gkoulemani, J. Hui, J.T.S. Irvine, L.A. Lawton, Aging microplastics enhances the adsorption of pharmaceuticals in freshwater, Science of The Total Environment, 912 (2024) 169467.

[78] G. Jaria, M.A.O. Lourenço, C.P. Silva, P. Ferreira, M. Otero, V. Calisto, V.I. Esteves, Effect of the surface functionalization of a waste-derived activated carbon on pharmaceuticals' adsorption from water, Journal of Molecular Liquids, 299 (2020) 112098.

[79] M.A. Islam, M.A. Chowdhury, M.S.I. Mozumder, M.T. Uddin, Langmuir Adsorption Kinetics in Liquid Media: Interface Reaction Model, ACS omega, 6 (2021) 14481.

[80] Y. Cui, Y. Tang, X. Wang, Template-free synthesis of graphitic carbon nitride hollow spheres for photocatalytic degradation of organic pollutants, Materials Letters, 161 (2015) 197.

[81] L. Shi, L. Liang, F. Wang, J. Ma, J. Sun, Polycondensation of guanidine hydrochloride into a graphitic carbon nitride semiconductor with a large surface area as a visible light photocatalyst, Catalysis Science & Technology, 4 (2014) 3235.

[82] P. Gibot, F. Schnell, D. Spitzer, Enhancement of the graphitic carbon nitride surface properties from calcium salts as templates, Microporous and Mesoporous Materials, 219 (2016) 42.

[83] S. Kumar, A. Baruah, S. Tonda, B. Kumar, V. Shanker, B. Sreedhar, Cost-effective and eco-friendly synthesis of novel and stable N-doped ZnO/g-C_3N_4 core–shell nanoplates with excellent visible-light responsive photocatalysis, Nanoscale, 6 (2014) 4830.

[84] M. Kim, S. Hwang, J.-S. Yu, Novel ordered nanoporous graphitic C_3N_4 as a support for Pt–Ru anode catalyst in direct methanol fuel cell, Journal of Materials Chemistry, 17 (2007) 1656.

[85] R. Bardestani, G.S. Patience, S. Kaliaguine, Experimental methods in chemical engineering: specific surface area and pore size distribution measurements—BET, BJH, and DFT, The Canadian Journal of Chemical Engineering, 97 (2019) 2781.

[86] T.A. Saleh, Chapter 3 - Kinetic models and thermodynamics of adsorption processes: classification, in: T.A. Saleh (Ed.) Interface Science and Technology, Elsevier 2022, pp. 65.

Appendix A. SEM and EDX analysis

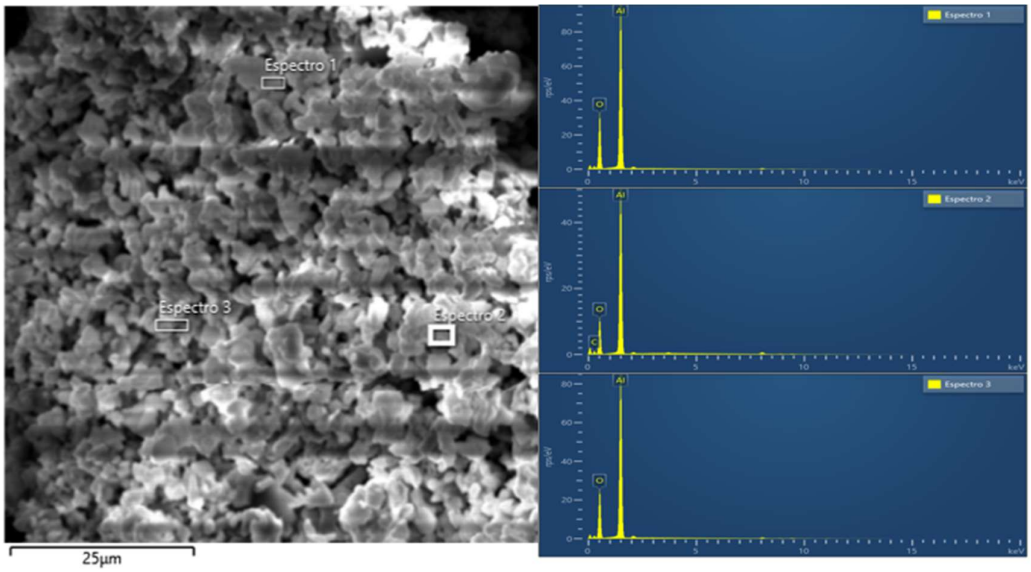

Figure A.1. Energy-dispersive X-Ray spectra (EDXS) of SEM for Bare spheres.

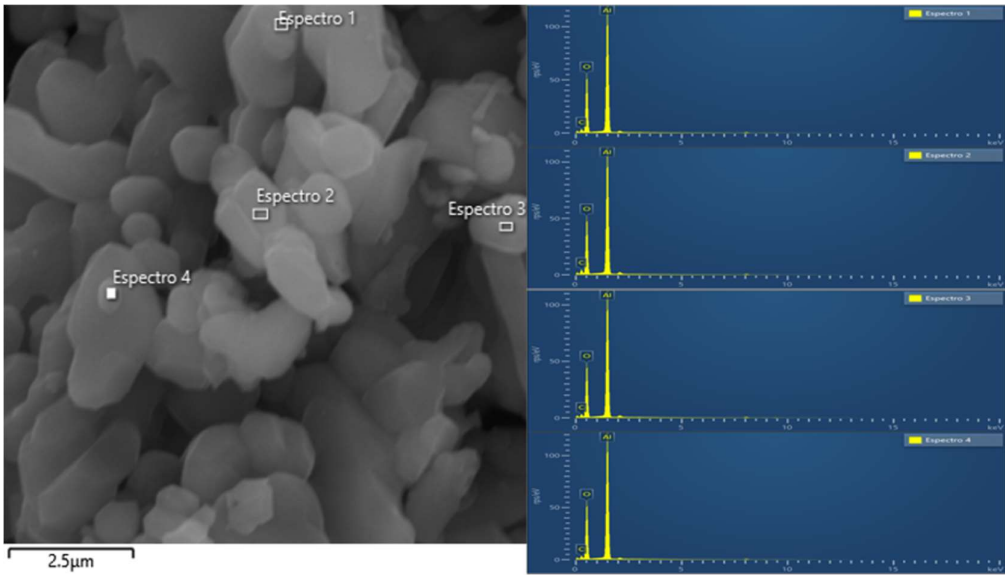

Figure A.2. Energy-dispersive X-Ray spectra (EDXS) of SEM for ACS/U_{25}.

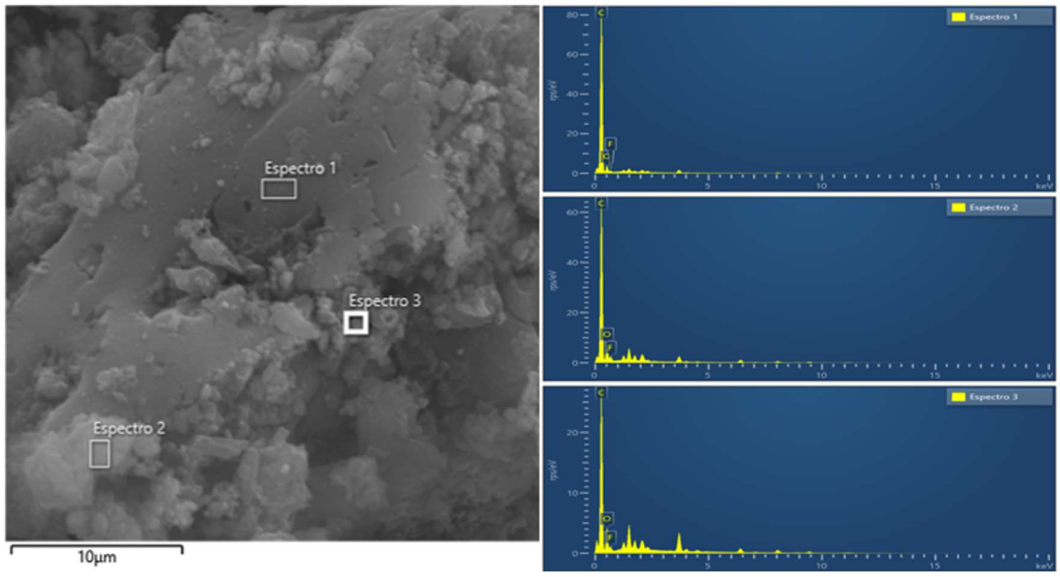

Figure A.3. Energy-dispersive X-ray spectra (EDXS) of SEM for AC_{MW}.

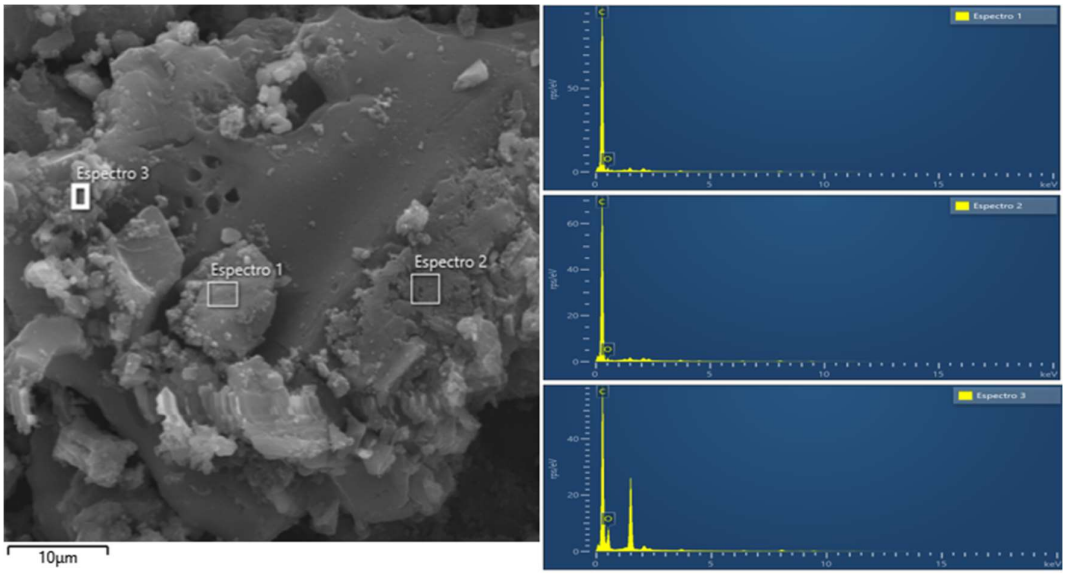

Figure A.4. Energy-dispersive X-ray spectra (EDXS) of SEM for AC/U_{25}.

Appendix B. Calibration curves

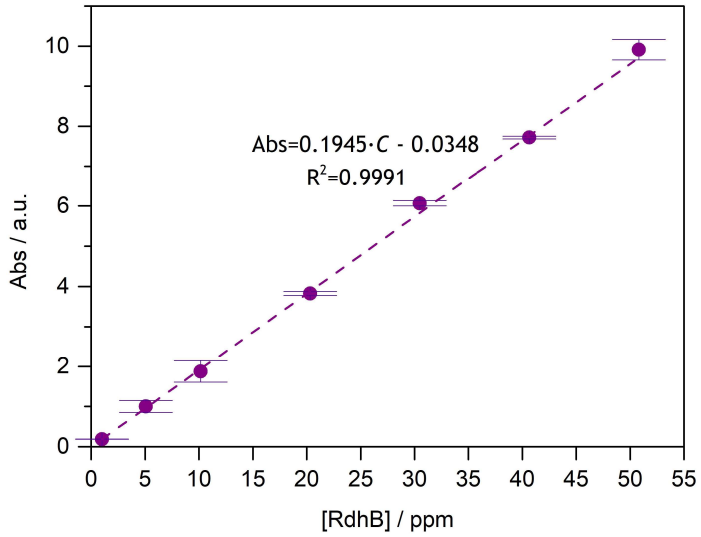

Figure B.1. Rhodamine B calibration curve for UV-Vis spectroscopy.

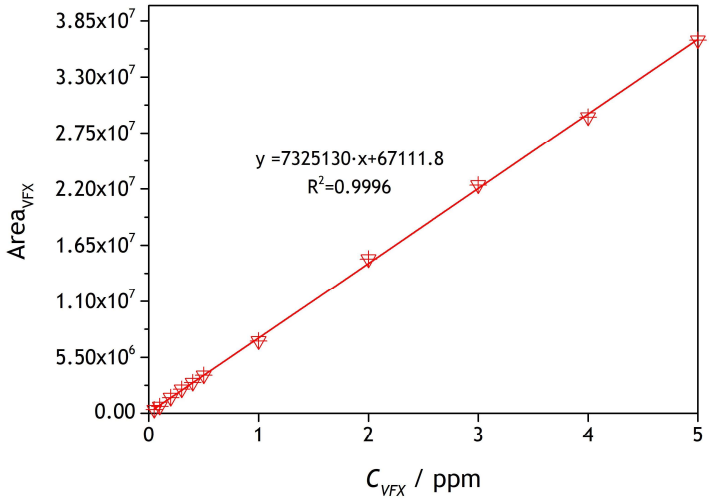

Figure B.2. VFX calibration curve for HPLC analysis.